UNIVERSITÀ DEGLI STUDI DI PADOVA

Dipartimento di Fisica e Astronomia "Galileo Galilei"

Master Degree in Physics

Final Dissertation

Shell shaped Bose-Einstein condensation in microgravity

Thesis supervisor

Prof. Luca Salasnich

Candidate

Irene Greghi

Academic Year 2019/2020

Contents

Introduction

In 1924 Satyendra Nath Bose derived the Planck law for black-body radiation in which he treated photons as a gas of identical particles [1] and he sent his paper to Albert Einstein which generalized Bose's theory [2] to an ideal gas of identical atoms having a conserved number of atoms and afterward he predicted that, at sufficiently low temperatures, atoms undergo a phase transition in which they form a macroscopic occupation of the lowest single-particle state of the system [3]. We know that this phenomenon, called Bose-Einstein condensation (BEC), happens for bosons, i.e. particles with a total spin that is an integer.

Since the theoretical prediction, it took seven decades before the condensation of bosonic particles (BEC) was directly observed in experiments. The delay is due to the fact that the formation of BEC requires high densities and extremely low temperatures of the order of the μK. In his work Einstein assumed a gas of identical non interacting particles and this led to the use of atoms of hydrogen in the attempt to achieve BEC due to their weak interatomic interactions. Around 1990, it was understood by Wieman [4] and his group that alkali atoms were a better candidate to achieve BEC [5] thanks to the fact that they lent themselves to laser cooling and, once they are trapped, it is also possible to further lower their temperature by means of evaporative cooling since they have a higher rates of elastic scattering, which are essential for this technique.

In 1995, by means of different cooling techniques, the experimental teams of Cornell and Wieman at Boulder and of Ketterle at MIT were able reach the temperatures and the densities required to observe BEC in vapours of ^{87}Rb [6] and ^{23}Na [7]and BEC in vapours of ^{7}Li were also reported [8]. The temperatures at which BEC were observed were of order 0.5—2 μK, depending on the alkali atom used and the atomic density achieved in the trap.

Through the years the study of ultracold gases has become a rising area of research that merges several disciplines such us atomic and molecular physics, quantum optics, statistical mechanics and condensed matter physics. Since its first observation BEC has been achieved in many atomic species, so far, behind the ones mentioned above, it has been realized also in ^{41}K as well as in spin-polarized H and metastable ^{4}He, and a huge number of experimental and theoretical groups worldwide is working in this field.

In 2017 the first Bose-Einstein condensate in space has been created on board the sounding rocket mission MAIUS-1 (Matter-Wave Interferometry in Microgravity) with ^{87}Rb atoms. Several experiment central to matter-wave interferometry were conducted during the six minutes of in-space flight, indeed thanks to the microgravity conditions it is possible to perform experiments with extended free-fall times, this results in a large enhancement in sensitivity of measures of inertial forces with matter-wave interferometers [9].

Historically, the study of quantum ultracold atomic gases has been characterized

by explorations of geometry, dimensionality, topology and interaction. Many properties has been discovered by expanding space of dimensionality and geometry, e.g. studying BEC in 2D has yielded insight into quasi-condensation and the BKT transition, exploring toroidal condensates has driven progress in understanding persistent current [12].

An interesting configuration to study, due to its distinctive topology, is a shell geometry in which the condensate would be confined to the surface of a spherical or ellipsoidal shell. The study of this configuration allows us to have a better understanding on how quantum mechanics works in curved geometries, on the transition of a condensate to a hollow shell from a conventional topology [10], on vortices behaviour [11], on how large we can make BECs while preserving their properties and on the properties of condensates in the ultradilute limit.

A BEC in the shape of a shell is inaccessible on the Earth, in fact due to gravitational effects atoms would fall at the bottom of the trap. The realization and exploration of this configuration is one of the ongoing investigation [12] aboard NASA CAL (Cold Atom Lab [13], [14]), a facility for the study of ultra-cold quantum gases in the microgravity environment, launched to the International Space Station (ISS) in 2018. This orbital BEC machine enables research in a temperature regime below 100 pK unlocking the potential to observe new quantum phenomena and has enabled quantum-gas experiments in a regime of perpetual freefall.

A series of experiments employing a bubble-trap is expected to investigate the physics of closed BEC shells, in particular, the proposal of Zobay and Garraway [15, 16] is currently under investigation. Their method is based on the use of radio-frequency-induced adiabatic potentials to create shell- shaped BEC and the loading of atoms does not relies on incoherent processes, e.g. optical pumping, but is performed by adiabatically deforming a conventional magnetic trap.

Motivated by the expected realization of hollow condensate in microgravity conditions, we study a shell-shaped Bose-Einstein condensate.

This thesis is organized as follow. In Chapter 1 we introduce the bubble-trap potential proposed in the experimental procedure of Zobay and Garraway [15, 16] and we study for which values of the parameter it depends on it is possible to achieve a shell-shaped condensate. In particular we plot the bubble-trap potential for different values of the parameters in order to study their effects.

In Chapter 2 we begin by illustrating the semiclassical approximation which will be adopted throughout the paper. Within this approximation we study the total density profiles at the critical temperature of condensation of an ideal Bose gas of ^{87} Rb in a shell-shaped trap provided by the bubble-trap potential studied in the previous chapter. The density profiles are compared for all the different values of the parameters of the external potential that we considered in the previous chapter, moreover we also study the effect on these profiles of varying the critical temperature of condensation.

Afterwards, we compute the critical temperature as a function of the total number of atoms in the gas trapped in a spherical shell and in an ellipsoidal shell. Finally, also the validity of the semiclassical approximation is studied and a representation of the condensate fraction as a function of the temperature is given.

Finally in Chapter 3 we study a dilute gas of strongly interacting bosons in a shell-shaped trap. We begin by introducing the formalism to described such a gas,

in particular we treat the interaction in the mean-field approximation by considering the Hartree-Fock theory in which we consider the thermal atoms as non interacting bosons in a self- consistent mean-field generated by the interaction with other atoms. Within this approximation we compute the total density using an iterative procedure, this allows us to calculate the critical temperature of condensation as a function of the total number of atoms of the trapped gas, then we compare the results with the ones we obtained for the ideal gas.

Afterwards we compute the thermal density and the condensate density at temperature lower than the critical one and we plot the corresponding density profiles. Finally, we compute the condensate fraction and the thermal one for a gas in a shell-shaped trap and we compare the results with the ones obtained for an ideal gas having the same number of atoms in the same trapping configuration.

Chapter 1

The bubble-trap potential

In this chapter we introduce the bubble-trap potential proposed in the experimental procedure of Zobay and Garraway [15, 16] currently under investigation [12] and we study for which values of the parameters it depends on it is possible to achieve a shell-shaped condensate, namely for which values of the parameter the atoms are confined to the surface of a sphere or of an ellipsoid.

1.1 The bubble-trap potential

Let us consider a system of ^{87}Rb atoms in the hyperfine state $|F = 2, m_F = 2\rangle$, confined in the three-dimensional harmonic potential:

$$u(\vec{r}) = \frac{m}{2}(\omega_x^2 x^2 + \omega_y^2 y^2 + \omega_z^2 z^2) \tag{1.1}$$

where m is the atomic mass, $\vec{\omega} = (\omega_x, \omega_y, \omega_z)$ are the frequencies of the confinement, and $\vec{r} = (x, y, z)$.

According to the procedure of Zobay and Garrawy [15,16] a shell-shaped condensate is achievable by properly tuning a radio frequency external field with a detuning $\Delta = \hbar\omega_{rf} - \Delta\epsilon(0)$, where ω_{rf} is the frequency of the rf field and $\Delta\epsilon(0)$ is the energy difference between two subsequent hyperfine levels at the center of the trap (i.e at the minimum of the magnetic field). The interaction between the rf radiation and a set of hyperfine levels, in a microgravity environment, results in the following bubble-trap potential:

$$U(\vec{r}) = 2\sqrt{\left[\frac{u(\vec{r})}{2} - \hbar\Delta\right]^2 + (\hbar\Omega)^2} \tag{1.2}$$

this provide a trapping potential shell for the atoms, i.e. a potential where the atoms are confined to the surface of a sphere or an ellipsoid, in the case in which the Rabi frequency Ω between the hyperfine levels is sufficiently strong and if the detuining Δ is much larger than Ω [12].
Note that since the Rabi frequency between sublevels differ, Ω is chosen to be the

Rabi freqeuncy between $M_F = 1$ and $M_F = 2$.

Let us consider the spherical case in which the frequencies of the harmonic trap are equal along the three directions, namely $\omega_x = \omega_y = \omega_z = \omega$, in particular we choose $\omega = 2\pi \times 100$ Hz. Therefore the 3D harmonic potential reduces to: $u(\vec{r}) = m\omega^2 \vec{r}^{\,2}/2$.

We want to work with effective dimensionless quantities, to do so we introduce some characteristic quantities, in particular we consider the frequency of the confinement $\omega = 2\pi \times 100$ Hz as the characteristic frequency, the other characteristic quantities are

$$\begin{aligned} &\text{characteristic length} \quad l_0 = \sqrt{\frac{\hbar}{m\omega}} = 1.088 \times 10^{-6}\text{m} \\ &\text{characteristic energy} \quad E_0 = \frac{\hbar^2}{m l_0^2} = \hbar\omega = 6.632 \times 10^{-32}\text{J} \\ &\text{characteristic temperature} \quad T_0 = \frac{\hbar\omega}{k_B} = 4.8604 \times 10^{-9}\text{K} \end{aligned} \tag{1.3}$$

then by using dimensionless units, namely: $\tilde{r} = r/l_0$, $\tilde{E} = E/E_0$, $\tilde{T} = T/T_0$ and $\tilde{n} = n/l_0^3$, we obtain the following adimensional bubble- trap potential

$$\tilde{U}(\vec{r}) = 2\sqrt{\left[\frac{1}{4}\tilde{r}^{\,2} - \tilde{\Delta}\right]^2 + \tilde{\Omega}^{\,2}} \tag{1.4}$$

In order to have a better understanding on the effects of the parameters $\tilde{\Delta}$ and $\tilde{\Omega}$ of the external potential we compare the adimensional bubble-trap potential $\tilde{U}(\tilde{r})$ for different values of these parameters. In particular we proceed by fixing one of the two parameters and by varying the other one, namely we will consider the following cases: $\tilde{\Delta} = 0$ with $\tilde{\Omega} = \{0, 20, 50, 70\}$, $\tilde{\Delta} = 70$ with $\tilde{\Omega} = \{0, 25, 50, 70\}$ and $\tilde{\Omega} = 50$ with $\tilde{\Delta} = \{0, 25, 100, 300\}$.

Since we are considering the spherical case, i.e. the frenquency of the confinement is the same along the three directions $\omega_x = \omega_y = \omega_z = \omega$, we will employ spherical coordinates $(\tilde{r}, \theta, \phi)$.

Harmonic confinement

For comparison we start by considering the harmonic confinement which is obtained by setting in the expression (1.4) of the adimensional bubble-trap potential $\tilde{U}(\tilde{r})$ the parameters $\tilde{\Delta} = \tilde{\Omega} = 0$.

By doing so the external potential reduces to the following adimensional harmonic potential

$$\tilde{U}(\tilde{r}) = \frac{1}{2}\tilde{r}^2 \tag{1.5}$$

A representation of this potential as a function of the rescaled radius $\tilde{r}$ is shown in Fig.(1.1), as we can see the potential has a minimum at the origin $\tilde{r} = 0$.

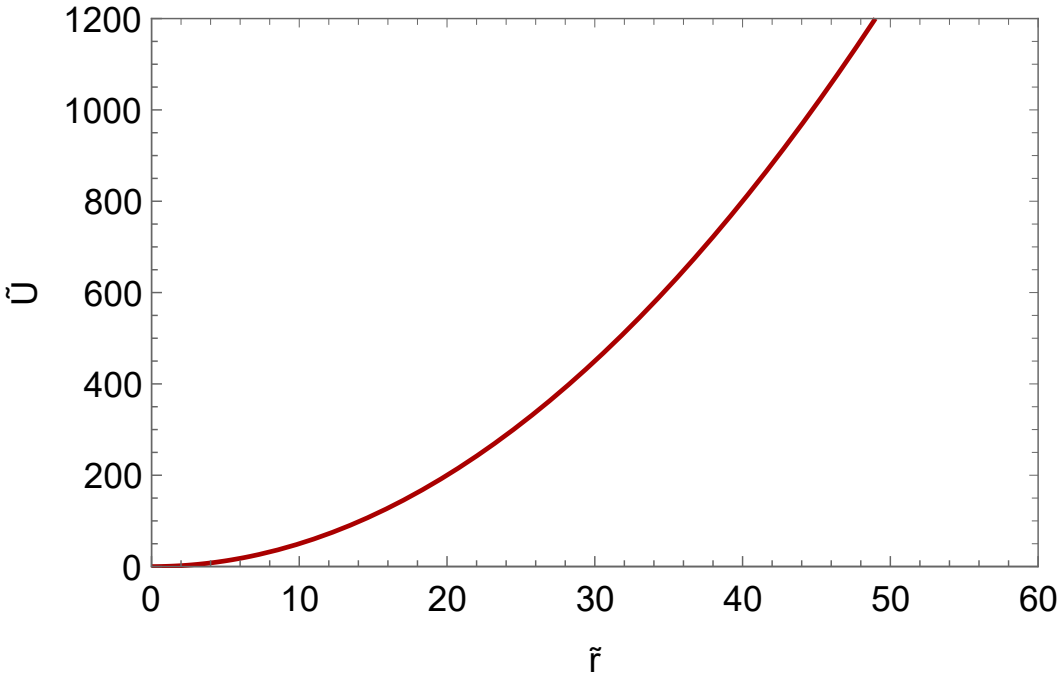

Figure 1.1: Dimensionless harmonic potential, obtained setting $\tilde{\Delta} = \tilde{\Omega} = 0$ in the equation for the dimensionless bubble-trap potential (1.4) as a function of the rescaled units $\tilde{r}$.

$$\tilde{\mathbf{\Delta}} = \mathbf{0}, \quad \tilde{\mathbf{\Omega}} = \{\mathbf{0}, \mathbf{20}, \mathbf{50}, \mathbf{70}\}$$

We proceed by fixing the detuning $\tilde{\Delta} = 0$ and by varying the Rabi frequency $\tilde{\Omega}$, in particular we will consider $\tilde{\Omega} = \{0, 20, 50, 70\}$. In this way we will have a better understanding on the effect of the parameter $\tilde{\Omega}$ on the adimensional bubble-trap potential $\tilde{U}(\tilde{r})$ of Eq.(1.4) in which we set the detuning $\tilde{\Delta}$ to zero obtaining

$$\tilde{U}(\vec{r}) = 2\sqrt{\left[\frac{1}{4}\tilde{r}^{\,2}\right]^2 + \tilde{\Omega}^{\,2}} \tag{1.6}$$

In Figure 1.2 we compare the profiles of the dimensionless bubble-trap potential $\tilde{U}(\tilde{r})$ of Eq.(1.6) for the different values of the parameter $\tilde{\Omega}$ which are expressed in units of the characteristic energy $E_0 = 6.632 \times 10^{-32}$ J defined in (1.3).

As shown in the figure, the potential $\tilde{U}(\tilde{r})$ has its minimum in the origin at $\tilde{r} = \tilde{r}_0$ for all the different values of the parameter $\tilde{\Omega}$ that we are considering. On the other hand the value of the minimum of the potential $\tilde{U}(\tilde{r}_0)$ changes for different values of the parameter $\tilde{\Omega}$, in particular it increases as $\tilde{\Omega}$ is increased accordingly to: $min_{\vec{r}}\, U(\vec{r}) = 2\hbar\Omega = \ \mu_c$, therefore also the critical chemical potential μ_c, i.e. the value of the chemical potential μ at the critical temperature, increases as $\tilde{\Omega}$ is increased.

Finally also the curvature of the potential changes as the Rabi frequency $\tilde{\Omega}$ changes, in particular from the figure we can see that by increasing the value of the parameter $\tilde{\Omega}$ the potential gets flatter in the region near the origin and the dimension of this region is control by $\tilde{\Omega}$, indeed it is larger for bigger values of $\tilde{\Omega}$.

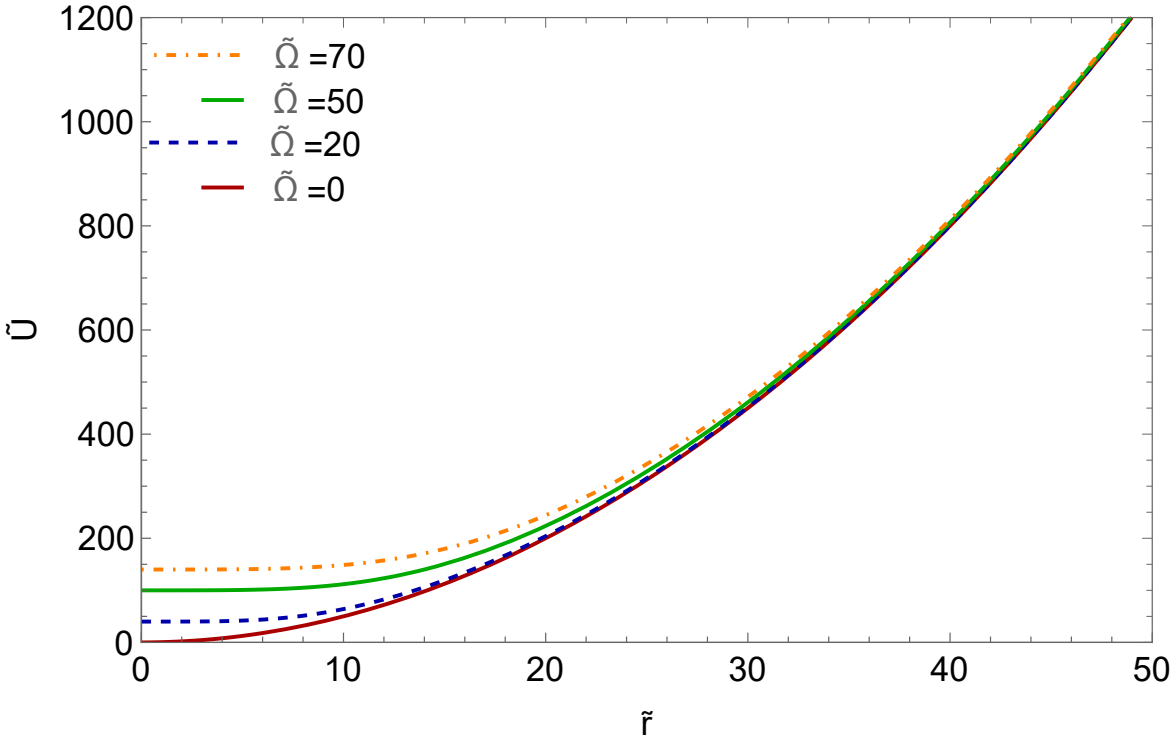

Figure 1.2: Dimensional potential $\tilde{U}(\tilde{r})$ as a function of the rescaled radius $\tilde{r}$. The plots are obtained using equation (1.4) for the adimensonal potential with the parameter $\tilde{\Delta}$ equal zero and for different values of the parameter $\tilde{\Omega}$: 0 (red line), 20 (blue dashed line), 50 (green line) and 70 (yellow dot dashed line). Here the potentials are in units of the characteristic energy $E_0 = 6.632 \times 10^{-32}$ J, the radius is in units of the characteristic length $l_0 = 1.088 \times 10^{-6}$ m and the parameters $\tilde{\Delta}$ and $\tilde{\Omega}$ are in units of E_0. The characteristics quantities are defined in Eq.(1.3.)

$$\tilde{\Delta} = 70, \quad \tilde{\Omega} = \{0, 25, 50, 70\}$$

We proceed by fixing the detuning $\tilde{\Delta} = 70$ and by varying the Rabi frequency $\tilde{\Omega}$, in particular we will consider $\tilde{\Omega} = \{0, 25, 50, 70\}$. This will allow us to have a better understanding on the effects of the parameters $\tilde{\Delta}$ and $\tilde{\Omega}$ on the adimensional bubble-trap potential $\tilde{U}(\tilde{r})$ of Eq.(1.4) which in this case becomes

$$\tilde{U}(\vec{r}) = 2\sqrt{\left[\frac{1}{4}\tilde{r}^{\,2} - 70\right]^2 + \tilde{\Omega}^{\,2}} \tag{1.7}$$

In Figure 1.3 we compare the profiles of the dimensionless bubble-trap potential $\tilde{U}(\tilde{r})$ of Eq.(2.19) for the different values of the parameter $\tilde{\Omega}$ which are expressed in units of the characteristic energy $E_0 = 6.632 \times 10^{-32}$ J defined in (1.3).

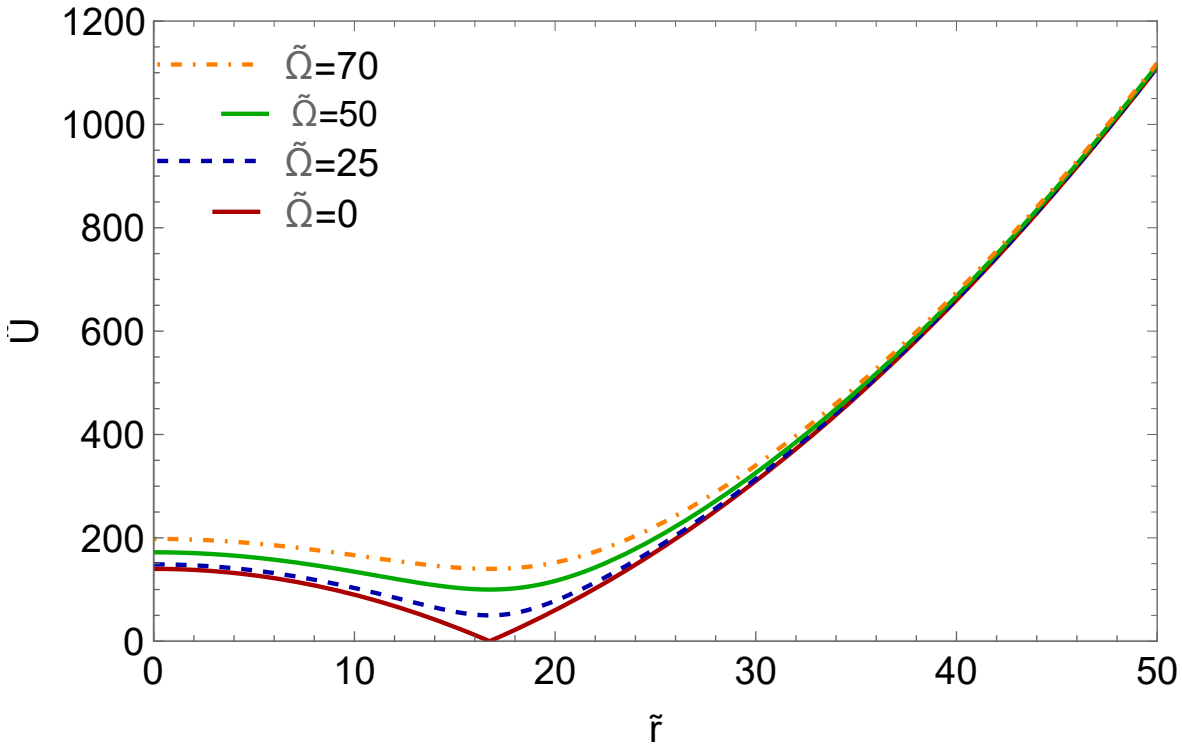

Figure 1.3: Dimensional potential $\tilde{U}(\tilde{r})$ as a function of the rescaled radius $\tilde{r}$. The plots are obtained using equation (1.4) for the adimensonal potential with the parameter $\tilde{\Delta} = 70$ and for different values of the parameter $\tilde{\Omega}$: 0 (red line), 20 (blue dashed line), 50 (green line) and 70 (yellow dot dashed line). Here the potentials are in units of the characteristic energy $E_0 = 6.632 \times 10^{-32}$ J, the radius is in units of the characteristic length $l_0 = 1.088 \times 10^{-6}$ m and the parameters $\tilde{\Delta}$ and $\tilde{\Omega}$ are in units of E_0. The characteristics quantities are defined in Eq.(1.3.)

As shown in the figure, the minimum of the potential, for all the different values

of the parameter $\tilde{\Omega}$ that we are considering, is no more in the origin as it was in the previous case in which we set $\tilde{\Delta} = 0$. The minimum of the potential is indeed found at $\tilde{r}_0 = 2\sqrt{\tilde{\Delta}}$ and it is therefore the same for all the different values of $\tilde{\Omega}$ that we are considering.

On the other hand the value of the minimum of the potential $\tilde{U}(\tilde{r}_0)$ changes for different values of the parameter $\tilde{\Omega}$, in particular it increases as $\tilde{\Omega}$ is increased accordingly to $min_{\vec{r}}\, U(\vec{r}) = 2\hbar\Omega = \ \mu_c$, therefore also the critical chemical potential μ_c, i.e. the value of the chemical potential μ at the critical temperature, increases as $\tilde{\Omega}$ is increased.

Finally, similarly to what we found in the previous case where we set $\tilde{\Delta} = 0$, we can see that also in this case the curvature of the potential is controlled by the Rabi frequency $\tilde{\Omega}$ changes. In particular we have that by increasing the value of this parameter $\tilde{\Omega}$ the potential gets flatter in the region near the minimum and the dimension of this region is control by the parameter $\tilde{\Omega}$, in particular it is larger for bigger values of $\tilde{\Omega}$ as we can see from Fig.(1.3).

$\tilde{\mathbf{\Omega}} = \mathbf{50}, \quad \tilde{\mathbf{\Delta}} = \{\mathbf{0}, \mathbf{25}, \mathbf{100}, \mathbf{300}\}$

Finally we fix the parameter $\tilde{\Omega} = 50$, a realistic value for this parameter [12], then we consider different values of the detuning $\tilde{\Delta}$, in particular we will consider $\tilde{\Delta} = \{0, 25, 100, 300\}$. In this way we will have a better understanding of the effects on the adimensional bubble-trap potential of the parameters $\tilde{\Omega}$ and especially on $\tilde{\Delta}$, which was kept fixed in the previous analyses. The equation (1.4) for the bubble-trap potential in this case becomes

$$\tilde{U}(\vec{r}) = 2\sqrt{\left[\frac{1}{4}\tilde{r}^{\ 2} - \tilde{\Delta}\right]^2 + 50^{\ 2}} \tag{1.8}$$

In Figure 1.4 we compare the profiles of the dimensionless bubble-trap potential $\tilde{U}(\tilde{r})$ of Eq.(1.8) for the different values of the parameter $\tilde{\Delta}$ which are expressed in units of the characteristic energy $E_0 = 6.632 \times 10^{-32}$ J defined in (1.3).

As shown in the figure, the value of the radius $\tilde{r}_0$ at which the adimensional potential $\tilde{U}(\tilde{r})$ is minimum varies for the different values of the parameter $\tilde{\Delta}$ that we are considering, indeed we found that the minimum point is given by $\tilde{r}_0 = 2\sqrt{\tilde{\Delta}}$. In other words, the minimum moves away from the origin for increasing value of the parameter $\tilde{\Delta}$ and therefore the parameter $\tilde{\Delta}$ acts to control the radius of the shell.

On the other hand the value of the potential on the minimum point $\tilde{r}_0$ does not depend on the parameter $\tilde{\Delta}$ but only on $\tilde{\Omega}$ since $\tilde{U}(\tilde{r}_0) = 2\tilde{\Omega}$ and it is therefore the same for all the cases that we are considering. Also the critical chemical potential μ_c, i.e. the value of the potential at the critical temperature T_c, is the same for all the cases since $min_{\vec{r}}\, U(\vec{r}) = 2\hbar\Omega = \ \mu_c$.

Finally, we can see that for values of the parameter $\tilde{\Delta}$ grater than zero the adimensional potential $\tilde{U}(\tilde{r})$ has a local maximum in the origin, moreover the value of this maximum increases as $\tilde{\Delta}$ is increased. As will be described in more detail in the following chapter, this behaviour will allow us to approximate, for large value of the parameter $\tilde{\Delta}$, the bubble-trap potential $\tilde{U}(\tilde{r})$ near its minimum at $\tilde{r} = \tilde{r}_0$, by a radially shifted harmonic trap [10].

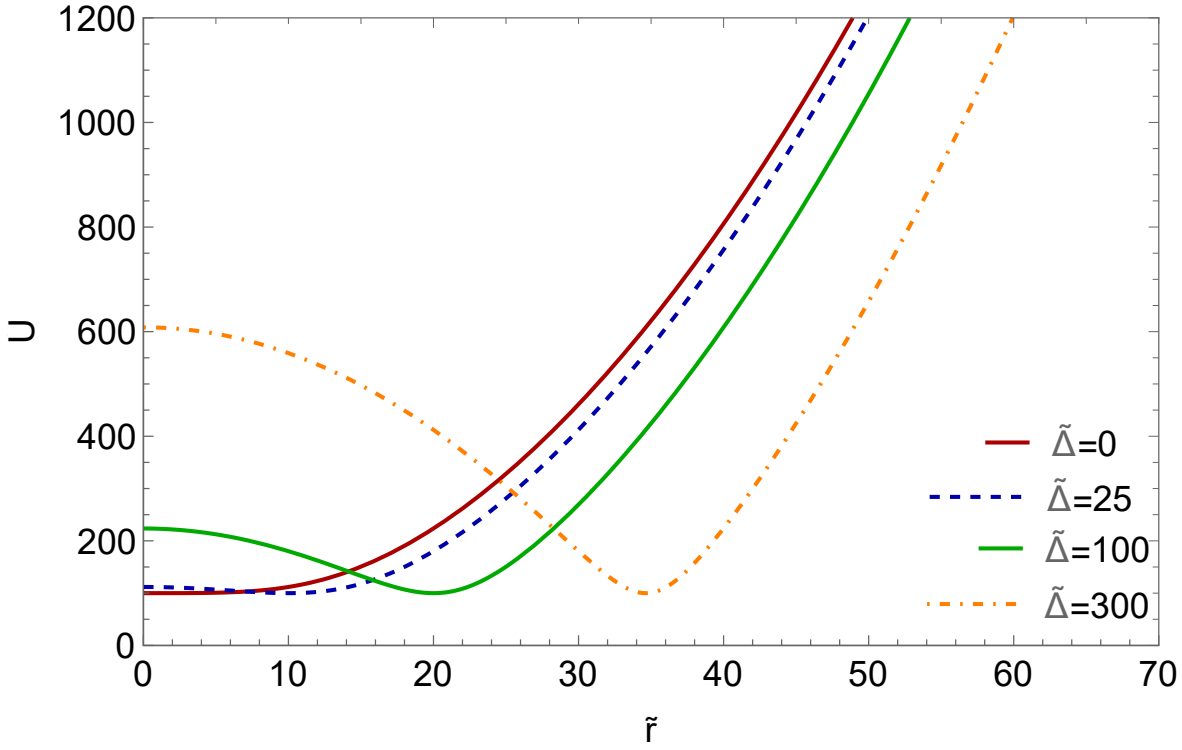

Figure 1.4: Dimensional potential $\tilde{U}(\tilde{r})$ as a function of the rescaled radius $\tilde{r}$. The plots are obtained using equation (1.4) for the adimensonal potential with the parameter $\tilde{\Omega} = 50$ and for different values of the parameter $\tilde{\Delta}$: 0 (red line), 25 (blue dashed line), 100 (green line) and 300 (yellow dot dashed line). Here the potentials are in units of the characteristic energy $E_0 = 6.632 \times 10^{-32}$ J, the radius is in units of the characteristic length $l_0 = 1.088 \times 10^{-6}$ m and the parameters $\tilde{\Delta}$ and $\tilde{\Omega}$ are in units of E_0. The characteristics quantities are defined in Eq.(1.3.)

To summarize, from this analysis we found that, for a fixed value of the detuning $\tilde{\Delta}$, varying the parameter $\tilde{\Omega}$ leads to a change in the curvature of the potential near the minimum at $\tilde{r}_0 = 2\sqrt{\tilde{\Delta}}$ as shown in Fig. 1.2 and Fig. 1.3. In particular we found that bigger values of the parameter $\tilde{\Omega}$ correspond to a flatter potential in the region near the minimum, moreover also the dimension of this region increases with the parameter $\tilde{\Omega}$.

As we will show in the next chapter, to a potential which is flatter in the region near the minimum corresponds a wider total density profile which goes to zero, moving

away from its maximum at $\tilde{r} = \tilde{r}_0$, more slowly with respect to a profile density that correspond to a less flat potential.

Therefore the parameter $\tilde{\Omega}$ serves the purpose of controlling the curvature of the minimum of the potential. From the literature we know that the Rabi frequency $\tilde{\Omega}$, through sufficiently large magnitude, ensures the stability against non adiabatic losses in the experimental procedure to achieve a shell-shaped condensate and a realistic value for this parameter, in units of the characteristic energy $E_0 = 6.632 \times 10^{-32}$ J, is $\tilde{\Omega} = 50$ [12]. The characteristic energy is defined in Eq.(1.3).

Furthermore, for a fixed value of the Rabi frequency $\tilde{\Omega}$, we found that by varying the detuning $\tilde{\Delta}$ the minimum $\tilde{U}(\tilde{r}_0)$ of adimensional bubble-trap potential of Eq.(1.4) moves away from the origin for increasing values of the parameter, according to $\tilde{r}_0 = 2\sqrt{\tilde{\Delta}}$ as shown in Fig. 1.4.

The value of the minimum of the potential $\tilde{U}(\tilde{r}_0)$ does not depend on the detuning $\tilde{\Delta}$ but only on $\tilde{\Omega}$, since $min_{\tilde{r}}\tilde{U}(\tilde{r}) = 2\tilde{\Omega}$ and so the parameter $\tilde{\Delta}$ acts to control the dimension of the bubble.
Besides we have found that, when the parameter $\tilde{\Delta}$ is greater than zero, which implies that the minimum of the potential is outside the origin at $\tilde{r}_0 = 2\sqrt{\tilde{\Delta}}$, the bubble-trap potential has a local maximum in the origin as shown in Fig. 1.3 and Fig. 1.4. Moreover, the value of this local maximum $\tilde{U}(0)$, increases for bigger values of $\tilde{\Delta}$. Hence for large values of the parameter $\tilde{\Delta}$ we have a more deep well centered in the minimum of the potential at $\tilde{r} = \tilde{r}_0$.

Chapter 2

Thermodynamics of a shell-shaped ideal Bose gas

In this chapter we start by illustrating the semiclassical approximation which will be adopted throughout the paper. Within this approximation we study the density profiles at the critical temperature of condensation of an ideal Bose gas of ^{87} Rb in a shell-shaped trap given by the bubble-trap potential studied in the previous chapter. The density profiles are compared for the different values of the parameters of external potential that we have considered in the previous chapter, moreover we also study the effect on these profiles of varying the critical temperature of condensation.

Afterwards, we compute the critical temperature of condensation as a function of the total number of atoms in the gas trapped in a spherical shell and in an ellipsoidal shell. Finally, also the validity of the semiclassical approximation is studied and a representation of the condensate fraction as a function of the temperature is given.

2.1 The semiclassical approximation

Let us consider an ideal Bose gas at finite temperature in a trap given by the external potential $U(\vec{r})$. In the framework of the grand canonical ensamble the number of particles in the quantum state $|\alpha\rangle$ with energy ϵ_α, where α represents a set of quantum numbers, is given by the thermal Bose distribution [17]:

$$N_\alpha = \frac{1}{e^{\beta(\epsilon_\alpha - \mu)} - 1} \tag{2.1}$$

where $\beta = 1/k_B T$ and μ is the chemical potential fixed by the total number of particles $N = \sum_\alpha N_\alpha$. Note that the difficulty lies on finding the quantized discrete energy levels $\{\epsilon_\alpha\}$ for a given external potential $U(\vec{r})$.

Let us write the total number of particles as

$$N = N_0 + N_T \tag{2.2}$$

where N_0 in the number of condensed particles and N_T is the number of particles out of the condensate.

We know that for temperatures lower than the critical temperature T_c of the transition $T \leq T_c$ the chemical potential μ is equal to lowest energy state $\mu = \epsilon_0$, while for $T \geq T_c$ there are no particles in the condensate and thus $N_0 = 0$. Note that these are approximations which become exact in the thermodynamic limit, i.e. $N \to \infty$. Therefore at $T = T_c$ the total number of particle N is:

$$N = \sum_{\alpha \neq 0} N_\alpha = \sum_{\alpha \neq 0} \frac{1}{e^{(\,\epsilon_\alpha - \epsilon_0)/k_B T_c} - 1} \tag{2.3}$$

from this expression one can gets the critical temperature T_c which is a function of the total number of particles N and of the energy levels $\{\epsilon_\alpha\}$, i.e. $T_c = f(N, \{\epsilon_\alpha\})$.

The semiclassical approximation [20] consists in considering, instead of the discrete quantized energy ϵ_α, the classical single particle energy, namely

$$\epsilon(\vec{r}, \vec{p}) = \frac{p^2}{2m} + U(\vec{r}) \tag{2.4}$$

while the quantum nature of the system is preserved by considering the Bose-Einsten distribution [17]

$$N_\alpha = \frac{1}{e^{\;\beta\;(\epsilon(\vec{r},\vec{p}) - \mu)} - 1} \tag{2.5}$$

in other words, we consider a quantum statistical mechanics in which the energy spectrum is continuous. For this approach to be valid the temperature T must be large compared with $\Delta\epsilon_\alpha / k_B$ where $\Delta\epsilon_\alpha$ denotes the separation between neighbouring energy levels.

This allows us to replace sums over states by integrals over the phase space, i.e. $\sum_{\alpha \neq 0} \to \int d^3\vec{r}\, d^3\vec{p}/(2\pi\hbar)^3$, therefore in this approximation the number of non condensed (thermal) particles N_T is now given by

$$N_T = \int \frac{d^3\vec{r}\, d^3\vec{p}}{(2\pi\hbar)^3} \frac{1}{e^{\beta(\frac{p^2}{2m} + U(\vec{r}) - \mu)} - 1} \tag{2.6}$$

this notation is useful also because it enables to introduce a thermal local density in the the real space $n_T(\vec{r})$ and in the reciprocal space $n_T(\vec{p})$ which are such that

$$N_T = \int d^3\vec{r}\; n_T(\vec{r}) = \int d^3\vec{p}\; n_T(\vec{p}) \tag{2.7}$$

where

$$n_T(\vec{r}) = \int \frac{d^3\vec{p}}{(2\pi\hbar)^3} \frac{1}{e^{\;\beta(\frac{p^2}{2m} + U(\vec{r}) - \mu)} - 1} \tag{2.8}$$

$$n_T(\vec{p}) = \int \frac{d^3\vec{r}}{(2\pi\hbar)^3} \frac{1}{e^{\,\beta(\frac{p^2}{2m}+U(\vec{r})-\mu)} - 1} \tag{2.9}$$

moreover in the Bose-Einstein distribution the dependence on the momentum $\vec{p}$ is explicit thus it is possible to integrate over the reciprocal space. By employing spherical coordinates we obtain the following expression for thermal density in the $\vec{r}$ space $n_T(\vec{r})$:

$$n_T(\vec{r}) = \frac{1}{\lambda_T^3} g_{3/2}(z(\vec{r})) = \frac{1}{\lambda_T^3} g_{3/2}(e^{\beta\,(\mu - U(\vec{r}))}) \tag{2.10}$$

where $z(\vec{r}) = e^{\,\beta\,(\mu - U(\vec{r}))}$ is the local fugacity, $\lambda_T = (2\pi\hbar^2\beta/m)^{1/2}$ is the thermal wave length and finally $g_{3/2}$ is the Bose function, an integral function defined as follow [17]

$$g_n(z) = \frac{1}{\Gamma(n)} \int_0^\infty d\eta\, \frac{z\,\eta^{n-1} e^{-\eta}}{1 - z\,e^{-\eta}} \tag{2.11}$$

Moreover for $|z| < 1$, $g_n(z)$ can also be written as $g_n(z) = \sum_{i=1}^{\infty} z^i/i^n$.

Note that if we consider the harmonic confinement, i.e. $U(\vec{r}) = m\omega^2 r^2/2$, the usual results [18, 19] are found. Indeed, according to what we found above the total number of non condensed particles N_T is:

$$N_T = \int d^3\vec{r}\; n_T(\vec{r}) = \int d^3\vec{r}\; \frac{1}{\lambda_T^3} g_{3/2}(e^{\beta\,(\mu - \frac{1}{2}m\omega^2 r^2)}) \tag{2.12}$$

from this expression we can derive the critical temperature

$$T_c = \frac{\hbar\omega}{k_B} \frac{1}{g_3(1)^{1/3}} N^{1/3} \tag{2.13}$$

and also the condensed fraction $N_0/N = 1 - (T/T_c)^3$.

2.2 Density profiles

In the previous section we have derived the thermal density $n_T(\vec{r})$ for an ideal trapped Bose gas within the semiclassical approximation and we obtained the expression of Eq.(2.10). We now want to use rescaled adimensional quantities, by mean of the characteristic quantites introduced in (1.3) the expression for the adimensional thermal density becomes

$$\tilde{n}_T(\tilde{r}) = \left(\frac{\tilde{T}}{2\pi}\right)^{\frac{3}{2}} g_{3/2}\left(e^{(\tilde{\mu}-\tilde{U}(\tilde{r}))/\tilde{T}}\right) \tag{2.14}$$

where the thermal density is units of l_0^3 with the characteristic length $l_0 = 1.088\times10^{-6}$ m, the temperature is in units of $T_0 = 4.860 \times 10^{-9}$ K, the chemical potential and the external potential are in units of $E_0 = 6.632 \times 10^{-32}$ J.

Let us now consider a system of non interacting ^{87}Rb atoms trapped by the bubble-trap potential namely we consider as the external potential appearing in the expression of the thermal density of Eq.(2.14) the bubble-trap potential $\tilde{U}(\tilde{r})$ of Eq. (1.4) that we have introduced and studied in the previous chapter.

At the critical temperature of condensation $T = T_c$ there are no particles in the condensate, i.e. $N_0 = 0$, moreover the chemical potential μ is equal to the minimum of the external potential, thus for the bubble-trap potential we have $\mu_c = \ min_r\, U(\vec{r}) = 2\hbar\Omega$. In rescaled adimensional units the expression becomes $\tilde{\mu}_c = \ min_{\tilde{r}}\, \tilde{U}(\tilde{r}) = 2\tilde{\Omega}$.

Therefore at the critical temperature $\tilde{T} = \tilde{T}_c$, the adimensional thermal density $\tilde{n}_T(\tilde{r})$ is equal to the total density $\tilde{n}(\tilde{r})$ of the system and, accordingly to what we said, it is given by

$$\tilde{n}(\tilde{r}) = \left(\frac{\tilde{T}_c}{2\pi}\right) g_{3/2}\left(e^{(2\tilde{\Omega}-\tilde{U}(\tilde{r}))/\tilde{T}_c}\right) \tag{2.15}$$

We now want to study the effects of varying the parameters $\tilde{\Delta}$ and $\tilde{\Omega}$ of the external potential, i.e. the bubble trap potential $\tilde{U}(\tilde{r})$ of Eq.(1.4), on the total density profiles $\tilde{n}(\tilde{r})$ given by Eq.(2.15) at the critical temperature of condensation $\tilde{T}_c$. In particular we will consider as the external potential the different bubble-trap potentials $\tilde{U}(\tilde{r})$ that we have studied and represented in the previous chapter, namely with $\tilde{\Delta} = 0$ with $\tilde{\Omega} = \{0, 20, 50, 70\}$, $\tilde{\Delta} = 70$ with $\tilde{\Omega} = \ \{0, 25, 50, 70\}$ and $\tilde{\Omega} = 50$ with $\tilde{\Delta} = \{0, 25, 100, 300\}$. For these different value of the parameters we represent the density profiles $\tilde{n}(\tilde{r})$ as a function of the rescaled radius $\tilde{r}$ for a fixed critical temperature $T_c = 50$ nK, besides as a comparison we will also consider the harmonic trap potential of Eq.(1.5).

Moreover, to show the effect of the critical temperature $\tilde{T}_c$ on the density profiles $\tilde{n}(\vec{r})$ we will represent the density profiles for fixed values of the parameters $\tilde{\Delta}$ and $\tilde{\Omega}$ by varying the critical temperature of condensation T_c.

Harmonic confinement

As a comparison we consider the case of an ideal Bose gas in a spherical harmonic confinement given by

$$\tilde{U}(\tilde{r}) = \frac{1}{2}\tilde{r}^2 \tag{2.16}$$

which is obtained by setting $\tilde{\Delta} = \tilde{\Omega} = 0$ in the expression (1.4) of the bubble-trap potential $\tilde{U}(\tilde{r})$, a representation of this potential is given in Fig. 1.1.

To show the effect of the critical temperature $\tilde{T}_c$ on the total density $\tilde{n}(\tilde{r})$ we plot in Fig. 2.1 the adimensional density profiles for different values of the critical temperature, in particular we consider $T_c = \{10, 25, 50, 100\}$ nK which in units of the characteristic temperature T_0 defined in (1.3) correspond to the adimensionless temperatures $\tilde{T}_c = \{2.08, 5.20, 10.40, 20.8\}$.

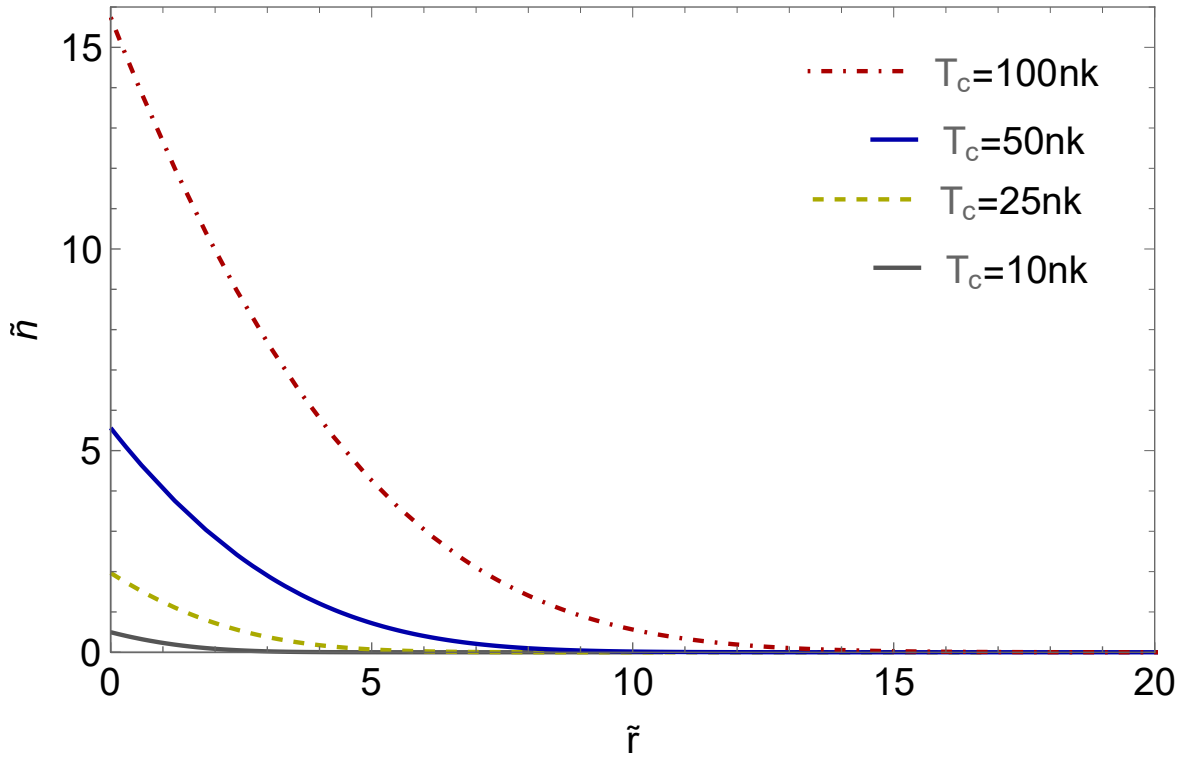

Figure 2.1: Dimensionless density profiles $\tilde{n}(\tilde{r})$ as a function of the scaled radius $\tilde{r}$ for different values of T_c.
The plot are obtained using the expression of the adimensional density of Eq.(2.15) considering the adimensional harmonic potential of Eq.(1.5) in which the parameters of the external potential $\tilde{\Delta}$ and $\tilde{\Omega}$ are zero. A representation of the potential is shown in figure (1.1). Here the density $\tilde{n}(\tilde{r})$ is unit of l_0^3 and the radius is in units of l_0, where $l_0 = 1.088 \times 10^{-6}$ m is the characteristic length defined in (1.3).

As we can see from the figure the total density profile $\tilde{n}(\tilde{r})$ has its maximum in the origin at $\tilde{r} = 0$ and the value of the maximum varies with the critical temperature T_c, in particular it increases as T_c is increased according to $\tilde{n}(0) = (\tilde{T}_c/2\pi)^{3/2}$.

The spherically symmetric harmonic trap of Eq.(1.5) that we are considering produces a fully filled spherical condensate. Moreover the density profile decreases, while moving away from the origin, more slowly for bigger value of the critical temperature T_c. As shown in the figure the total number of particles N, obtained by integrating

the total density $\tilde{n}(\tilde{r})$ over the space, increases as the critical temperatures T_c is increased, therefore also the dimension of the condensate increases by increasing the critical temperatures.

$\tilde{\Delta} = 0, \quad \tilde{\Omega} = \{0, 20, 50, 70\}$

Let us now proceed by fixing $\tilde{\Delta} = 0$ and by varying $\tilde{\Omega} = \{0, 20, 50, 70\}$ in the expression of the bubble-trap potential of Eq.(2.19), namely

$$\tilde{U}(\vec{r}) = 2\sqrt{\left[\frac{1}{4}\tilde{r}^{\,2}\right]^2 + \tilde{\Omega}^{\,2}}$$

which is represented as a function of the rescaled radius $\tilde{r}$ in Fig. 1.2.

We want to have a better understanding on the effects of the parameters $\tilde{\Delta}$ and $\tilde{\Omega}$ on the total density $\tilde{n}(\tilde{r})$ of Eq.(2.15), namely

$$\tilde{n}(\tilde{r}) = \left(\frac{\tilde{T}_c}{2\pi}\right) g_{3/2}\left(e^{(2\tilde{\Omega} - \tilde{U}(\tilde{r}))/\tilde{T}_c}\right) \tag{2.17}$$

to do so in Figure 2.2 we compare for a fixed critical temperature, $T_c = 50$ nK, the adimensional total density profiles $\tilde{n}(\tilde{r})$ for the different values of the parameters corresponding to the different adimensional potentials $\tilde{U}(\tilde{r})$ that we have consider and represented in Fig.1.2.

As we can see from figure 2.2 the total density profiles have the maximum in the origin at $\tilde{r} = 0$ which is the minimum point of the external potential $\tilde{U}(\tilde{r})$ as shown in Fig. 1.2. The maximum of the density $\tilde{n}(0)$ is the same for all the different values of the parameter $\tilde{\Omega}$ that we are considering, indeed the value of the adimensional density in the origin, i.e. the value of the maximum density, reduces to $\tilde{n}(0) = (\tilde{T}_c/2\pi)^{3/2}$ which does not depend on the parameter $\tilde{\Omega}$.

By setting $\tilde{\Delta} = 0$ we found the filled sphere condensate geometry as in the case of the harmonic confinement of Eq.(1.5) to which the bubble-trap potential of Eq.(2.19) reduces when also $\tilde{\Omega}$ is zero (red line).

From the figure we can see that the density profiles $\tilde{n}(\tilde{r})$ decrease, while moving away from the origin, more slowly for bigger values of the parameter $\tilde{\Omega}$. Moreover, the density profiles have a bigger width for bigger values of this parameter as a result of the different curvature of the corresponding bubble-trap potential $\tilde{U}(\tilde{r})$ shown in Fig. 1.2. We have indeed found that the parameter $\tilde{\Omega}$ acts to control the curvature of the bubble-trap potential $\tilde{U}(\tilde{r})$ near its minimum, in particular we have that for bigger values of $\tilde{\Omega}$ the bubble-trap potential is flatter in the region near the minimum and the dimension of this region gets larger for larger values of $\tilde{\Omega}$. As a result of this we have that for values of $\tilde{\Omega}$ greater than zero we have no more the cusp which is

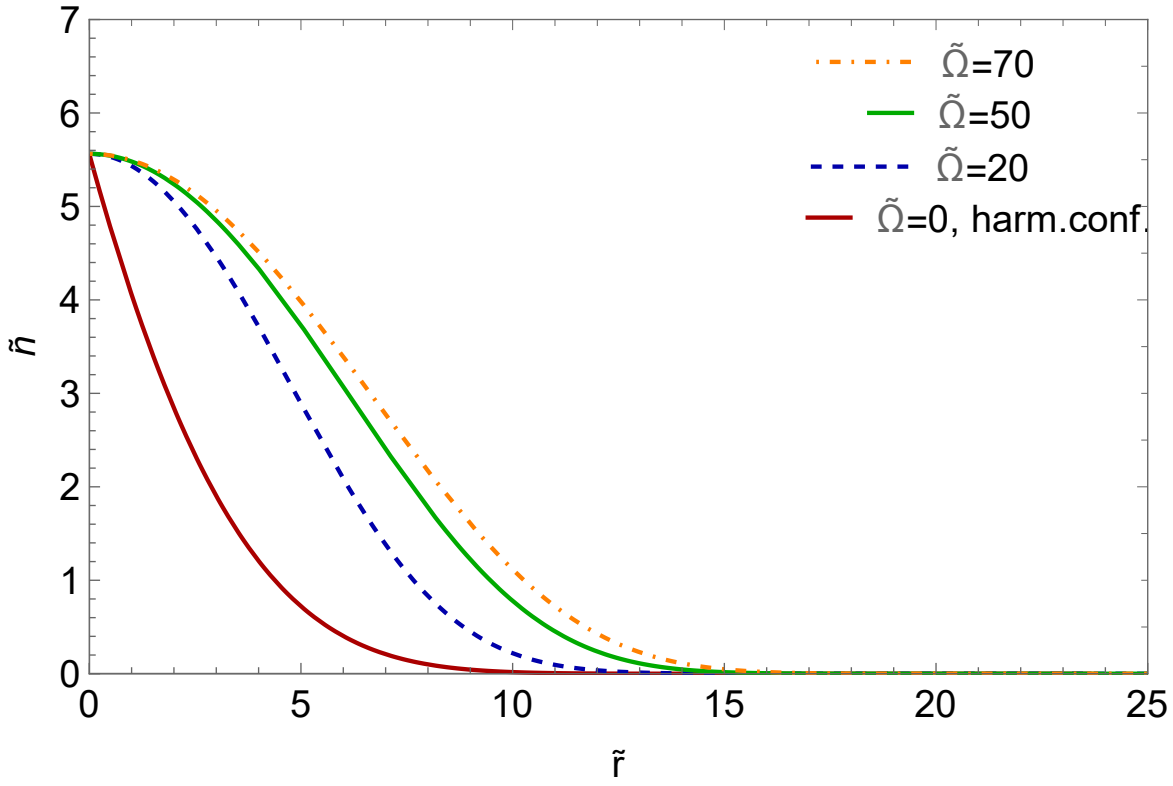

Figure 2.2: Adimensional density $\tilde{n}(\tilde{r})$ profiles as a function of the rescaled radius $\tilde{r}$ at a fixed critical temperature $T_c = 50$ nK. The plots are obtained using equation (2.15) for the adimensonal density in which we consider as the external potential the adimensional bubble-trap potential $\tilde{U}(\tilde{r})$ of Eq.(1.4) with the parameter $\tilde{\Delta}$ equal zero and for different values of the parameter $\tilde{\Omega}$: 0 (red line), 20 (blue dashed line), 50 (green line) and 70 (yellow dot dashed line). Here the densities are in units of l_0^3 with $l_0 = 1.088 \times 10^{-6}$ m, the radius is in units of the characteristic length l_0 and the parameters $\tilde{\Delta}$ and $\tilde{\Omega}$ are in units of E_0. The characteristics quantities are defined in Eq.(1.3).

instead present when $\tilde{\Omega}$ is zero, i.e. for the harmonic confinement.

Finally, in figure 2.3 we show the effect of varying the critical temperature T_c on the total density $\tilde{n}(\tilde{r})$, in particular we consider the case in which the parameters of the external adimensional bubble-trap potential of Eq.(2.19) are $\tilde{\Delta} = 0$ and $\tilde{\Omega} = 50$. We found that the total density profiles have the maximum at $\tilde{r}_0 = 0$ and the value of the maximum varies with the critical temperature T_c since $\tilde{n}(0) = (\tilde{T}_c/2\pi)^{3/2}$, therefore the value of the maximum increases as the critical temperature increases.

Moreover the density profiles decrease while moving away from the center of the trap, i.e. the origin, and the total number of atoms N in the system, obtained by integrating the density $\tilde{n}(\tilde{r})$ over the space, increases as the critical temperature T_c is increased and so does the dimension of the condensate.

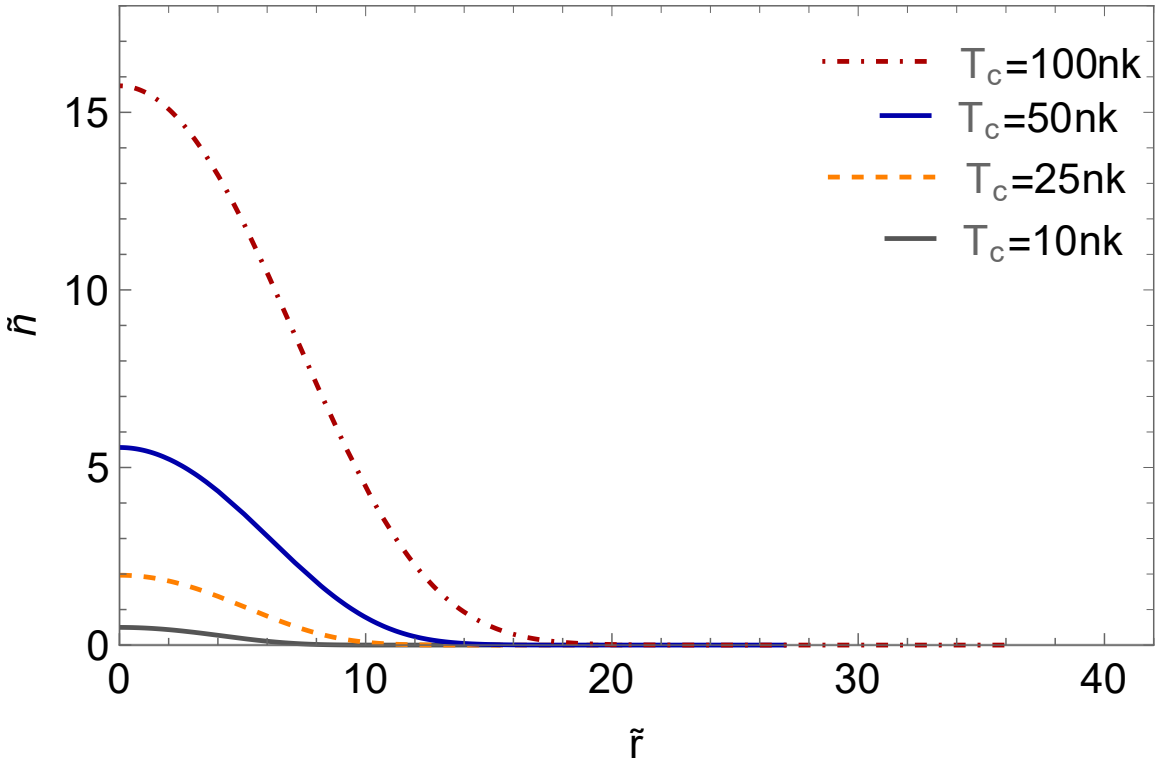

Figure 2.3: Adimensional density profiles $\tilde{n}(\tilde{r})$ as a function of the rescaled radius $\tilde{r}$. The plots are obtained using equation (2.15) for the adimensonal density in which we consider the adimensional potential $\tilde{U}(\tilde{r})$ of Eq.(1.4) with the parameters $\tilde{\Delta} = 0$ and $\tilde{\Omega} = 50$. The density profiles are compared for different values of the critical temperature T_c: 10nK (gray line), 25 nK (dashed yellow line), 50 nK (blue line) and 100 nK (dot-dashed red line). Here the densities are in units of l_0^3 with $l_0 = 1.088 \times 10^{-6}$ m, the radius is in units of the characteristic length l_0 and the parameter $\tilde{\Omega}$ is in unit of E_0. The characteristics quantities are defined in Eq.(1.3).

$$\tilde{\boldsymbol{\Delta}} = \mathbf{70}, \quad \tilde{\boldsymbol{\Omega}} = \{\mathbf{0}, \mathbf{25}, \mathbf{50}, \mathbf{70}\}$$

Let us now proceed by fixing $\tilde{\Delta} = 70$ and by varying $\tilde{\Omega} = \{0, 25, 50, 70\}$ in the expression of the bubble-trap potential of Eq.(1.7), namely

$$\tilde{U}(\tilde{r}) = 2\sqrt{\left[\frac{1}{4}\tilde{r}^{\,2} - 70\right]^2 + \tilde{\Omega}^{\,2}}$$

which is represented as a function of the rescaled radius $\tilde{r}$ in Fig.(1.3).

We want to have a better understanding on the effects of the parameters $\tilde{\Delta}$ and $\tilde{\Omega}$ on the density $\tilde{n}(\tilde{r})$ of Eq.(2.15), namely

$$\tilde{n}(\tilde{r}) = \left(\frac{\tilde{T}_c}{2\pi}\right) g_{3/2}\left(e^{\,(2\tilde{\Omega} - \tilde{U}(\tilde{r}))/\tilde{T}_c}\right) \tag{2.18}$$

to do so we proceed in the same way of the previous case, namely in Figure 2.4 we compare for a fixed critical temperature, $T_c = 50$ nK, the adimensional total density profiles $\tilde{n}(\tilde{r})$ of Eq.(2.15) for the various values of the parameter $\tilde{\Omega}$ that we are considering, namely for the different adimensional bubble- trap potentials $\tilde{U}(\tilde{r})$ that we have consider and represented in Fig.1.3.

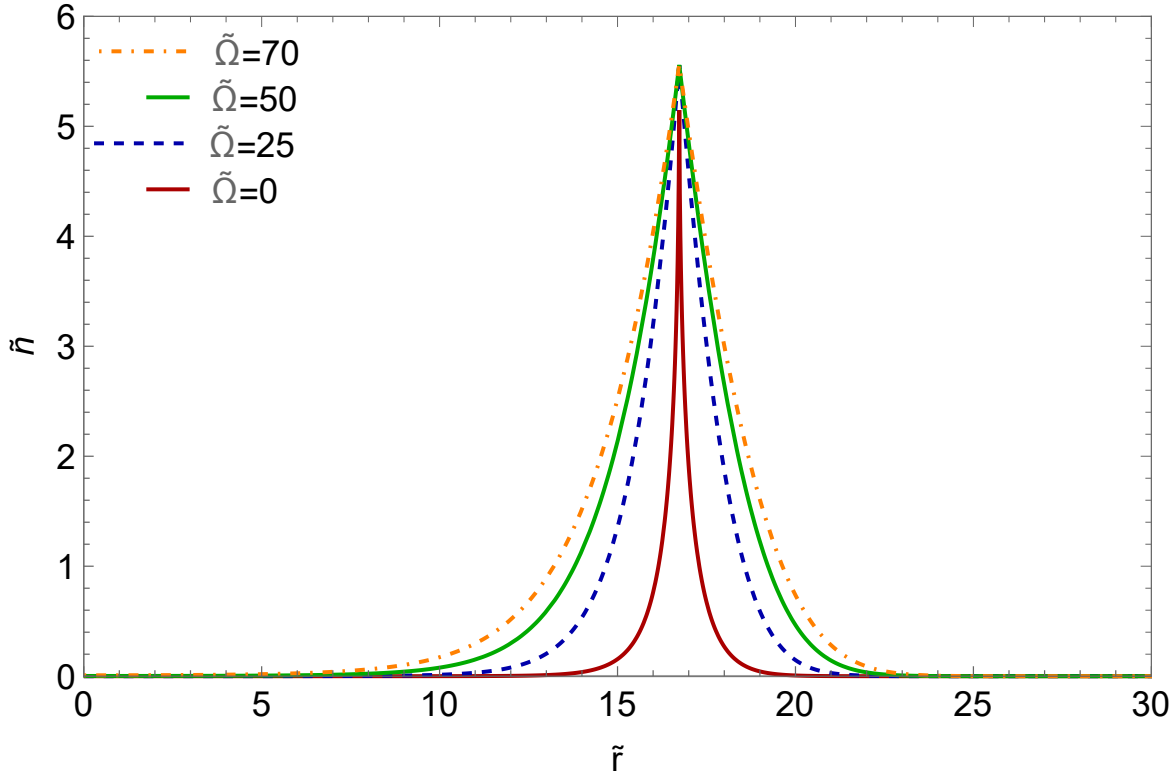

Figure 2.4: Dimensional density $\tilde{n}(\tilde{r})$ profiles as a function of the rescaled radius $\tilde{r}$ at a fixed critical temperature $T_c = 50$ nK. The plots are obtained using equation (2.15) for the adimensonal density in which we consider as the external potential the adimensional bubble-trap potential $\tilde{U}(\tilde{r})$ of Eq.(1.4) with the parameter $\tilde{\Delta} = 70$ and for different values of the parameter $\tilde{\Omega}$: 0 (red line), 20 (blue dashed line), 50 (green line) and 70 (yellow dot dashed line). Here the densities are in units of l_0^3 with $l_0 = 1.088 \times 10^{-6}$ m, the radius is in units of the characteristic length l_0 and the parameters $\tilde{\Delta}$ and $\tilde{\Omega}$ are in units of E_0. The characteristics quantities are defined in Eq.(1.3).

The total density profiles $\tilde{n}(\tilde{r})$ have the maximum at $\tilde{r}_0 = 2\sqrt{\tilde{\Delta}}$, which is the value of the radius at which the bubble-trap potential $\tilde{U}(\tilde{r})$ is minimum. As we can see from the figure he value of the maximum $\tilde{n}(\tilde{r}_0)$ is the same for all the different values of the parameter $\tilde{\Omega}$, indeed $\tilde{n}(\tilde{r}_0) = (\tilde{T}_c/2\pi)^{3/2}$ which does not depend on the parameter $\tilde{\Omega}$.

Moreover, as shown in the figure the width of the density profile $\tilde{n}(\tilde{r})$ increases with $\tilde{\Omega}$, in fact for small values of the parameter we have a narrow profile and the atoms are localized near the maximum, i.e. the center of the trap, while for bigger

values of the parameter $\tilde{\Omega}$ the density profile $\tilde{n}(\tilde{r})$ goes to zero more slowly and the atoms occupy a larger region.

In other words we have that for bigger values of the parameter $\tilde{\Omega}$ the density profile is more wide and therefore the value of the total density $\tilde{n}(\tilde{r})$ in the region near the origin, i.e. near $\tilde{r} = 0$, is bigger. This behaviour of the total density profiles $\tilde{n}(\tilde{r})$ is the result of the different curvature of the corresponding external bubble-trap potential near its minimum shown in fig. 2.4, where we found that for bigger values of $\tilde{\Omega}$ the potential is flatter in the region near the minimum and this region has a bigger dimension for bigger values of this parameter.

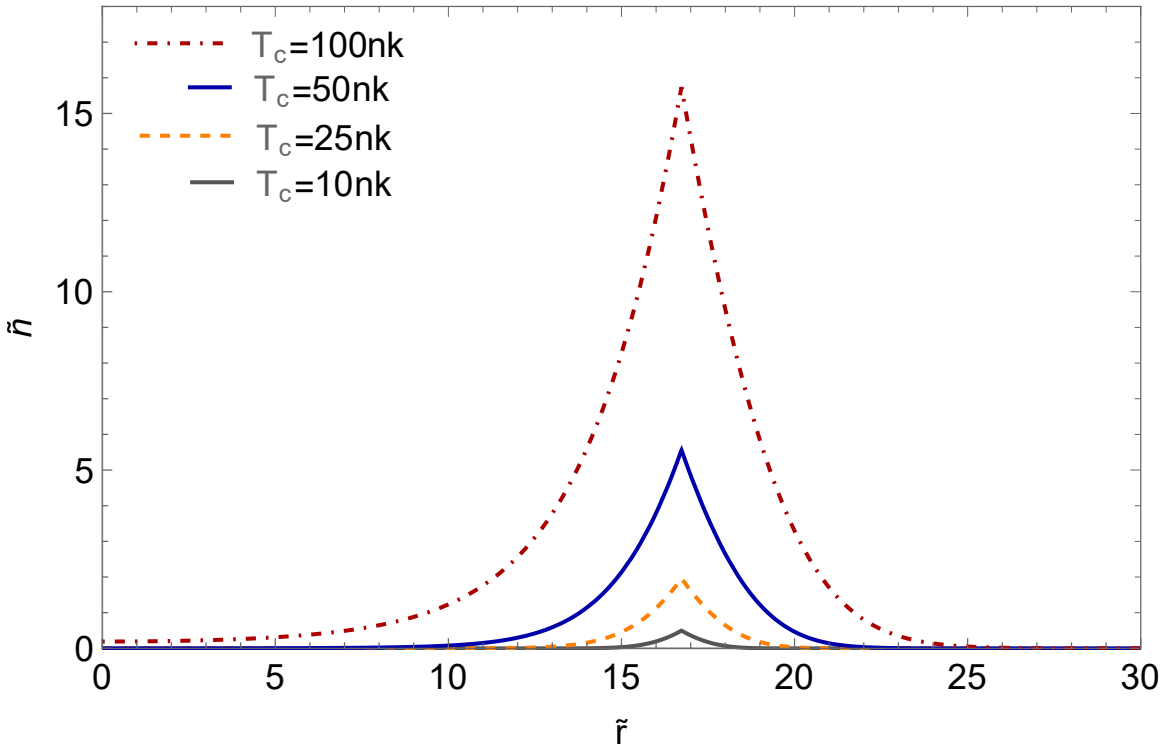

Figure 2.5: Adimensional density $\tilde{n}(\tilde{r})$ profiles as a function of the rescaled radius $\tilde{r}$ for different values of the critical temperature T_c: 10nk (gray line), 25nk (yellow dotted line), 50nk (blue line), 100nK (red dot-dashed line). The plots are obtained using equation (2.15) for the adimensonal density in which we consider the adimensional potential $\tilde{U}(\tilde{r})$ of Eq.(1.4) with the parameter $\tilde{\Omega} = 50$ and $\tilde{\Delta} = 70$. Here the densities are in units of l_0^3 with $l_0 = 1.088 \times 10^{-6}$ m, the radius is in units of the characteristic length l_0 and the parameters $\tilde{\Delta}$ and $\tilde{\Omega}$ are in units of E_0. The characteristics quantities are defined in Eq.(1.3)

Finally in Fig.2.5 we want to show the effect of varying the critical temperature T_c on the total density profile $\tilde{n}(\tilde{r})$, in particular we consider the case in which the parameters of the external adimensional bubble-trap potential $\tilde{U}(\tilde{r})$ are $\tilde{\Delta} = 70$ and $\tilde{\Omega} = 50$.

As said above the density profiles have the maximum outside the origin at $\tilde{r}_0 = 2\sqrt{\tilde{\Delta}}$ and the value of the maximum varies with the critical temperature, in particular we have $\tilde{n}(\tilde{r}_0) = (\tilde{T}_c/2\pi)^{3/2}$, therefore the value of the maximum increases as the critical temperature $\tilde{T}_c$ increases.

For the values of the parameter that we are considering, i.e. $\tilde{\Delta} = 70$ and $\tilde{\Omega} = 50$, the density profiles $\tilde{n}(\tilde{r})$ are wide and the atoms are not localized only in the region near the maximum but are instead spread also outside this region. Moreover, as shown in the plots in the figure the density profiles are not symmetric with respect to the maximum at $\tilde{r} = \tilde{r}_0$, indeed the total density $\tilde{n}(\tilde{r})$ for values of the adimensional radius $\tilde{r}$ smaller than the point of maximum $\tilde{r}_0$, i.e. near the origin, is bigger than the total density evaluated for values of the radius $\tilde{r}$ bigger than the point of minimum $\tilde{r}_0$.

The behaviour described above is more evident for bigger critical temperatures T_c, indeed as we can see from the figure, for example in the case of $T_c = 100$ nK, the value of the density $\tilde{n}(\tilde{r})$ near the origin is bigger with respect to the density $\tilde{n}(\tilde{r})$ at different critical temperatures.

Finally, the total number of atoms N of the ideal Bose gas, which is such to have as the critical temperature the one that we are considering, increases as the critical temperature T_c is increased. The total number of atoms N is obtained by integrating the total density $\tilde{n}(\tilde{r})$, at that critical temperature, over the space.

$\tilde{\Omega} = 50, \quad \tilde{\Delta} = \{0, 25, 100, 300\}$

Let us now proceed by fixing $\tilde{\Omega} = 50$ and by varying $\tilde{\Delta} = \{0, 25, 100, 300\}$ in the expression of the bubble-trap potential of Eq.(2.19), namely

$$\tilde{U}(\vec{r}) = 2\sqrt{\left[\frac{1}{4}\tilde{r}^{\,2} - \tilde{\Delta}\right]^2 + \tilde{\Omega}^{\,2}}$$

which is represented as a function of the rescaled radius $\tilde{r}$ in Fig.(1.4).

We want to have a better understanding on the effects of the parameters of the external potential $\tilde{\Omega}$ and especially $\tilde{\Delta}$, which was kept fixed in the previous analyses, on the density $\tilde{n}(\tilde{r})$ of Eq.(2.15), namely

$$\tilde{n}(\tilde{r}) = \left(\frac{\tilde{T}_c}{2\pi}\right) g_{3/2}\left(e^{\,(2\tilde{\Omega} - \tilde{U}(\tilde{r}))/\tilde{T}_c}\right)$$

to do so we compare in Figure 2.6 the density profiles $\tilde{n}(\tilde{r})$, at a fixed critical temperature $T_c = 50$ nK, for the different values of the parameters $\tilde{\Omega}$ and $\tilde{\Delta}$ mentioned above corresponding to the different adimensional bubble-trap potentials $\tilde{U}(\tilde{r})$ that we have considered and represented in Fig.1.4.

As shown in the figure the density profiles have the maximum at $\tilde{r} = \tilde{r}_0 = 2\sqrt{\tilde{\Delta}}$, which is the value of the radius where the potential is minimum. Hence the maximum moves away from the origin for increasing value of the parameter $\tilde{\Delta}$ and therfore the detuning $\tilde{\Delta}$ of the rf field acts to control the size of the shell which is bigger for bigger values of this parameter.

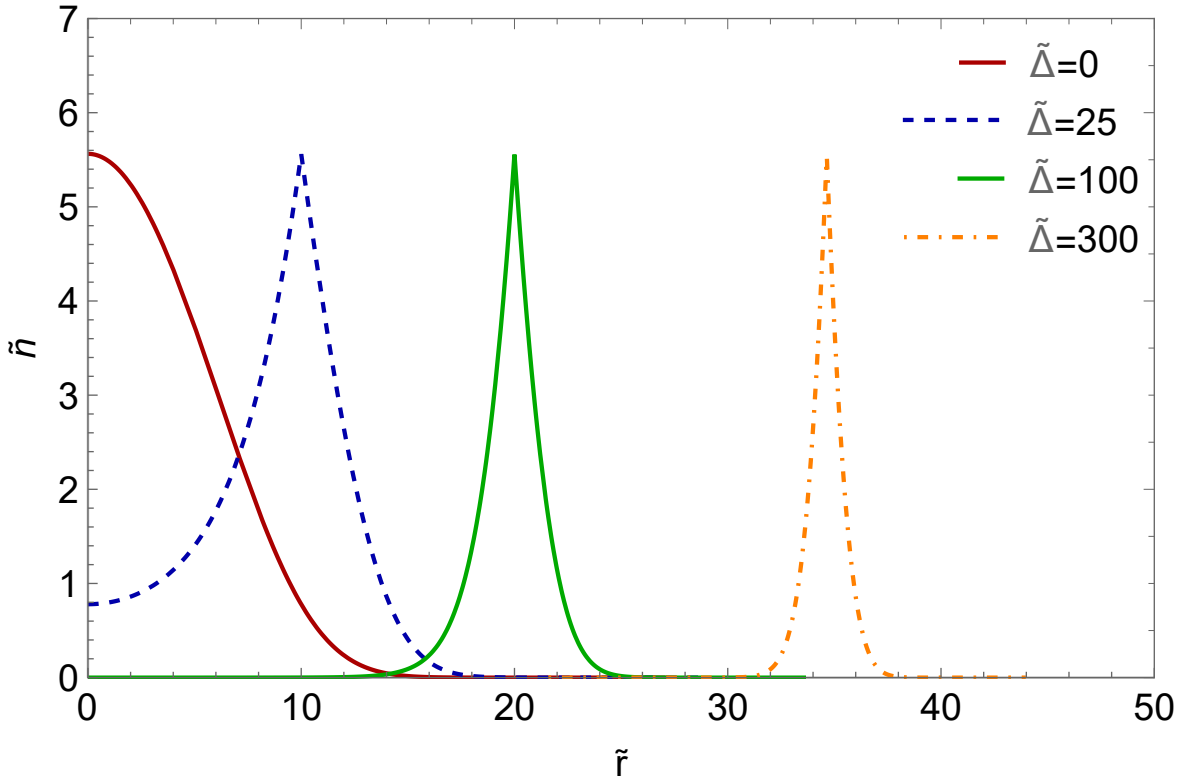

Figure 2.6: Dimensional density $\tilde{n}(\tilde{r})$ profiles as a function of the rescaled radius $\tilde{r}$ at a fixed critical temperature $T_c = 50$ nK. The plots are obtained using equation (2.15) for the adimensonal density in which we consider the adimensional potential $\tilde{U}(\tilde{r})$ of Eq.(1.4) with the parameter $\tilde{\Omega} = 50$ and for different values of the parameter $\tilde{\Delta}$: 0 (red line), 25 (blue dashed line), 100 (green line) and 300 (yellow dot dashed line). Here the densities are in units of l_0^3 with $l_0 = 1.088 \times 10^{-6}$ m, the radius is in units of the characteristic length l_0 and the parameters $\tilde{\Delta}$ and $\tilde{\Omega}$ are in units of E_0. The characteristics quantities are defined in Eq.(1.3).

On the other hand the value of the maximum is the same for all the different cases that we are considering since $\tilde{n}(\tilde{r}_0) = (\tilde{T}_c/2\pi)^{3/2}$, hence it does not depend on $\tilde{\Delta}$. Besides, we can see from the figure that the various values of the parameter $\tilde{\Delta}$ show the evolution of the condensate from the filled sphere condensate geometry obtainable for $\tilde{\Delta} = 0$, to a condensate having a small hollow region at its center for $\tilde{\Delta} = 100$ to the condensate in the thin spherical shell limit achievable for $\tilde{\Delta} = 300$.

We found that by increasing the detuning $\tilde{\Delta}$ of the applied rf field the value of the density $\tilde{n}(\tilde{r})$ in the origin becomes smaller and smaller until it is zero. Therefore, as said, increasing or decreasing the parameter $\tilde{\Delta}$, at a constant chemical potential $\mu_c = 2\tilde{\Omega}$, results in a deformation between the filled and the hollow condensate geometries. In other words, in order to have a shell-shaped condensate the detuning $\tilde{\Delta}$ the must be much larger than the parameter $\tilde{\Omega}$.

Moreover as we can see from the plots of the density profiles in the case of $\tilde{\Delta} = 100$ (green line) and $\tilde{\Delta} = 300$ (dot-dashed yellow line), for bigger values of the parameter $\tilde{\Delta}$ the width of the density profile $\tilde{n}(\tilde{r})$ reduces and we have a more narrow profile, hence it is possible to obtained different trapping configuration, from thicker shell

with a small size to thinner one with a larger size, by choosing increasing values of the parameter $\tilde{\Delta}$.

Finally, to show the effect of varying the critical temperature T_c on the density profile $\tilde{n}(\tilde{r})$ we plot in Fig. 2.7 the adimensional total density $\tilde{n}(\tilde{r})$ as a function of the radius for the case in which the parameters of the external bubble-trap potential $\tilde{U}(\tilde{r})$ of Eq.(1.8) are $\tilde{\Omega} = 50$ and $\tilde{\Delta} = 100$.

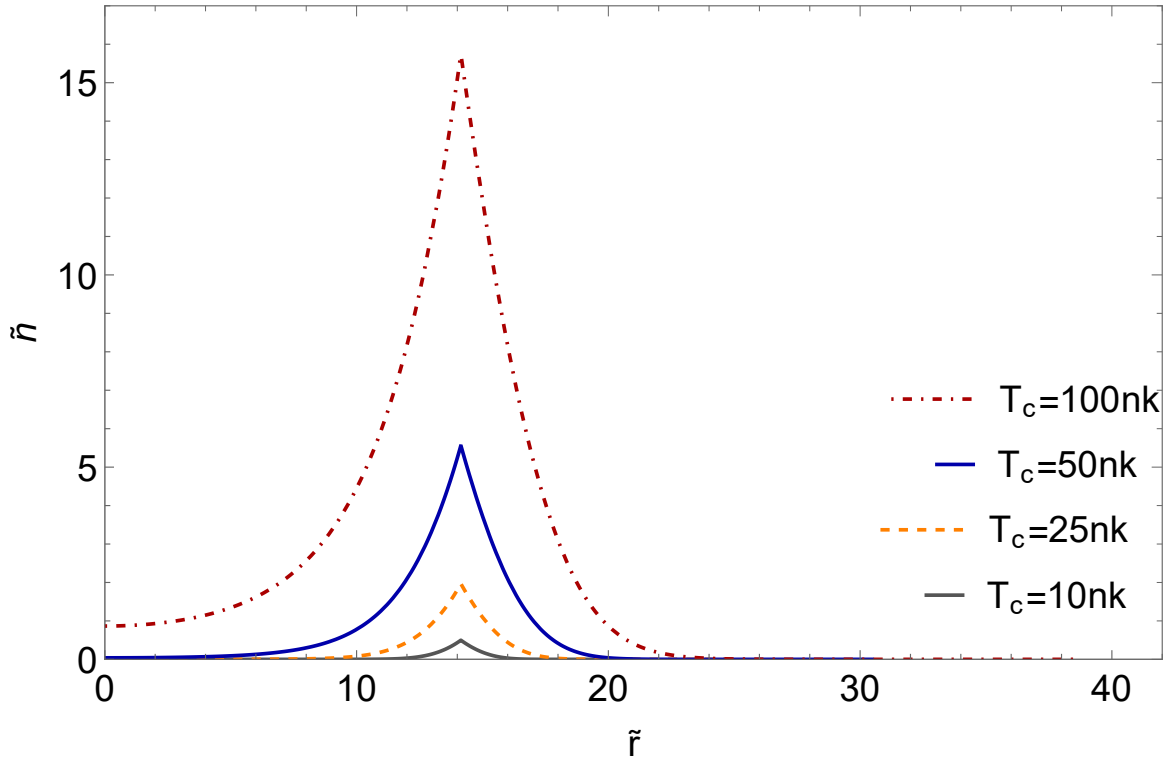

Figure 2.7: Dimensional density $\tilde{n}(\tilde{r})$ profiles as a function of the rescaled radius $\tilde{r}$ for different values of the critical temperature T_c: 10nk (gray line), 25nk (yellow dotted line), 50nk (blue line), 100nK (red dot-dashed line). The plots are obtained using equation (2.15) for the adimensonal density in which we consider the adimensional potential $\tilde{U}(\tilde{r})$ of Eq.(1.4) with the parameter $\tilde{\Omega} = 50$ and $\tilde{\Delta} = 100$. Here the densities are in units of l_0^3 with $l_0 = 1.088 \times 10^{-6}$ m, the radius is in units of the characteristic length l_0 and the parameters $\tilde{\Delta}$ and $\tilde{\Omega}$ are in units of E_0. The characteristics quantities are defined in Eq.(1.3)

As said above the maximum of the density is outside the origin at $\tilde{r}_0 = 2\sqrt{\tilde{\Delta}}$ and the values of the density in this point increases with the temperature according to $\tilde{n}(\tilde{r}_0) = (\tilde{T}_c/2\pi)^{3/2}$.

We can see form the figure that the density profile is not symmetric with respect to the maximum point $\tilde{r}_0$, indeed the total density $\tilde{n}(\tilde{r})$ has a bigger value at radius smaller than the maximum point $\tilde{r}_0$ than when it is evaluated at radius bigger than $\tilde{r}_0$. As shown by the plots in the figure this behaviour is more evident for bigger value of the critical temperature, i.e. $T_c = 100$ nK, for which we can see that the total

density $\tilde{n}(\tilde{r})$ near the origin is much bigger than zero.

Moreover for big value of the critical temperature of condensation $\tilde{T}_c$ the density profile $\tilde{n}(\tilde{r})$ is wider and hence the atoms are no more localized only in the region near the maximum but are instead spread also outside of this region in the manner described above.

As a consequence the total number of atoms N in the ideal Bose gas having a certain critical temperature $\tilde{T}_c$ increases for increasing values of $\tilde{T}_c$, where the total number of atoms N is obtained by integrating over the space the total density $\tilde{n}(\tilde{r})$ evaluated at that temperature.

To summarize the results obtained in this analysis: in the comparison shown in Fig. 2.3, Fig. 2.5 and Fig. 2.7 of the total density profiles $\tilde{n}(\tilde{r})$ for different critical temperatures $\tilde{T}_c$ at fixed values of the parameters of the external bubble-trap potential $\tilde{\Delta}$ and $\tilde{\Omega}$, and hence also at a constant chemical potential since $\mu_c = 2\hbar\Omega$, we found that the total number of atoms N of the ideal gas which is such to have a certain critical temperature $\tilde{T}_c$ increases as the critical temperature of condensation $\tilde{T}_c$ is increased. The total number of atoms N is obtained by integrating the total density $\tilde{n}(\tilde{r})$ of Eq.(2.15) over the space.

Moreover also the value of the maximum of the density at $\tilde{r} = \tilde{r}_0$, which is given by $\tilde{n}(\tilde{r}_0) = (T_c/2\pi)^{3/2}$, increases with the critical temperature and also the width of the density profiles $\tilde{n}(\tilde{r})$ increases with T_c, therefore the atoms are spread in a more large region around the point of maximum $\tilde{r}_0$ for bigger value of the temperature $\tilde{T}_c$.

Regarding the effects of the parameter $\tilde{\Omega}$, we have found in the previous chapter in Fig. 1.2 and in Fig. 1.3 that it serves the purpose to control the curvature of the potential near its minimum at $\tilde{r}_0$. This action results in density profiles $\tilde{n}(\tilde{r})$ which are wider for bigger values of $\tilde{\Omega}$ since for these values of the parameter the corresponding external bubble-trap potential $\tilde{U}(\tilde{r})$ presents a more large region, near its minimum at $\tilde{r} = \tilde{r}_0$, where the potential is flatter. The behaviour just described can be seen in Fig. 2.2 and in Fig. 2.4 where we plotted the density profiles $\tilde{n}(\tilde{r})$ at a fixed critical temperature $\tilde{T}_c$ for different values of $\tilde{\Omega}$.

Notice that since the value of the maximum density $\tilde{n}(\tilde{r}_0)$ is the same for the various values of $\tilde{\Omega}$ a wider density profile for bigger values of $\tilde{\Omega}$ implies a bigger total number of atoms N in the gas which is such to have as the characteristic temperature $T_c = 50$ nK.

Furthermore, we found that in order to obtain a shell-shaped condensate the detuning $\tilde{\Delta}$ must be much larger than the Rabi frequency $\tilde{\Omega}$, indeed as seen in Fig. 2.6 where we plot the total density profiles for $\tilde{\Omega} = 50$ kept fixed, by increasing the value of the parameter $\tilde{\Delta}$ the density $\tilde{n}(\tilde{r})$ near the origin at $\tilde{r} = 0$ reduces until it is zero. In other words increasing the parameter $\tilde{\Delta}$, at a constant chemical potential $\mu_c = 2\hbar\tilde{\Omega}$, results in a deformation from the filled condensate geometry (at $\tilde{\Delta} = 0$) to the hollow condensate geometry.

Finally the detuning $\tilde{\Delta}$ of the rf field acts to control the dimension of the shell-shaped condensate and its thickness, it is indeed possible to obtain different trapping configuration, from thicker shell with small size, obtained for $\tilde{\Delta} = 100$ to thinner ones with a larger size, obtained for $\tilde{\Delta} = 300$, by increasing $\tilde{\Delta}$ as shown in Fig. 2.6.

2.3 Critical temperature of an ideal bose gas

For a system of non interacting ^{87}Rb atoms in the hyperfine state $|F = 2, m_F = 2 >$ confined in the bubble-trap potential $\tilde{U}(\tilde{r})$ given by equation (1.4), we want to compute the critical temperature of the Bose condensation T_c as a function of the total number of atoms N in the ideal gas.

The total number of atoms N in the ideal Bose gas which is such to have a certain critical temperature $\tilde{T}_c$, within the semiclassical approximation described in section 2.1 and by adopting scaled units, is obtained by integrating over the space the adimesional total density $\tilde{n}(\tilde{r})$ found in Eq.(2.15), evaluated at the critical temperature $\tilde{T}_c$ that we are considering.

In this way we find the total number of atoms N in the ideal gas at the critical temperature of condensation $\tilde{T}_c$ that we are considering, namely the total number of atoms N is given by the following expression

$$N = \int d^3\tilde{r} \left(\frac{\tilde{T}_c}{2\pi}\right)^{\frac{3}{2}} g_{\frac{3}{2}} \left(e^{(2\,\tilde{\Omega} - \tilde{U}(\tilde{r}))/\tilde{T}_c}\right) \tag{2.19}$$

where we used the fact that, at the critical temperature of the condensation $\tilde{T} = \tilde{T}_c$, the dimensionless chemical potential $\tilde{\mu}_c$ is equal to the minimum of the external potential. So, in the case that we are considering where the gas is confined by the bubble-trapped potential $\tilde{U}(\tilde{r})$ of Eq.(1.4), the adimensional critical chemical potential is given by $\tilde{\mu}_c = min_{\,\tilde{r}} \tilde{U}(\tilde{r}) = 2\tilde{\Omega}$.

We are considering a spherical shell, namely the frequency of the harmonic confinement $u(\vec{r})$ introduced in Eq.(1.1) is the same along the three directions $\omega_x = \omega_y = \omega_z = \omega$, where the harmonic confinement is the one that traps the atoms before we apply the radio frequency field to deform the conventional trap into the a shell-shaped atomic trap described by the bubble-trap potential $\tilde{U}(\tilde{r})$ of Eq.(1.4) [15, 16].

Thanks to the symmetry of the system we employ spherical coordinates $(\tilde{r}, \theta, \phi)$, and so the expression for the total number of atoms becomes

$$N = 4\pi \int_0^\infty d\tilde{r}\; \tilde{r}^2 \left(\frac{\tilde{T}_c}{2\pi}\right)^{\frac{3}{2}} g_{\frac{3}{2}} \left(e^{\frac{1}{\tilde{T}_c}(2\,\tilde{\Omega} - \tilde{U}(\tilde{r}))}\right) \tag{2.20}$$

in which, due to the spherical symmetry, the integral over the solid angle is simply 4π.

We proceed by numerically integrating this expression for different values of the critical temperatures $\tilde{T}_c$, then we plot the number of atoms N obtained from the integration in the x-axis and the corresponding critical temperature $\tilde{T}_c$ in the y-axis. By doing so we obtain a representation of the critical temperature $\tilde{T}_c$ of the condensation as a function of the total number of atoms N in the ideal Bose gas.

According to the results obtained in the previous analyses on the effects of the parameters $\tilde{\Delta}$ and $\tilde{\Omega}$ on the bubble-trap potential $\tilde{U}(\tilde{r})$ and on the density profiles $\tilde{n}(\tilde{r})$, we will consider as the external potential the bubble-trap potential $\tilde{U}(\tilde{r})$ of Eq.(1.4)

with $\tilde{\Omega} = 50$, a realistic value for this parameter [12], and with $\tilde{\Delta} = \{100, 300\}$. With this values for the parameter the bubble-trap potential $\tilde{U}(\tilde{r})$ will provide a trapping potential shell for the atoms, i.e. a potential where the atoms are confined to the surface of the sphere. In particular the bubble-trap potential with $\tilde{\Delta} = 100$ correspond to a thicker shell with a small size and the one with $\tilde{\Delta} = 300$ to a thinner shell with a larger size as shown in Fig.(2.6).

Furthermore, as a comparison we also consider the harmonic confinement of Eq.(1.5), obtained by setting $\tilde{\Delta} = \tilde{\Omega} = 0$ in the expression of the adimensional bubble- trap potential $\tilde{U}(\tilde{r})$ of Eq.(1.4), for which we know the dependence of the critical temperature T_c on the total number of atoms N in the gas found in Eq.(2.13).

The critical adimensional temperature $\tilde{T}_c$ of condensation as a function of the number of atoms N in the gas is show in Fig. 2.8.

As we can see from figure 2.8, for a fixed total number of atoms N, the critical temperature $\tilde{T}_c$ for the thinner shell, i.e. with bubble-trap potential $\tilde{U}(\tilde{r})$ having $\tilde{\Delta} = 100$ (dashed green line), is slightly lower than the one for the thicker shell obtained with the bubble-trap potential having $\tilde{\Delta} = 300$ (dot-dashed blue line).

Moreover, we can see that, for a fixed number of atoms N in the gas, the critical temperature $\tilde{T}_c$ of a system of atoms in a conventional harmonic traps (red line) is much bigger than the one for a system in which we consider as the external potential $\tilde{U}(\tilde{r})$ the bubble-trap potential of Eq.(1.4), namely for the gas in a shell-shaped atomic trap.

In the experimental procedure proposed by Zobay and Garraway [15,16] and currently under investigation at CAL [12] a shell-shaped atomic trap is engineered by an adiabatic deformation, in a microgravity environment, of a conventional magnetic trap with a radiofrequency field. Therefore, since the quantum degeneracy is harder to reach in bubble-traps than in conventional harmonic traps, even if the atomic cloud cools during the adiabatic deformation of the trap, when the temperature in the predressed harmonic potential is not low enough an initial condensate may become a thermal cloud [22].

Let us now compute the condensed fraction N_0/N as a function of the adimensional temperature $\tilde{T}$ for the non interacting gas with $N = 1.6 \times 10^5$ atoms in a shell-shaped trap provided by the bubble-trap potential $\tilde{U}(\tilde{r})$ of Eq.(1.4) with the parameters $\tilde{\Delta} = 100$ and $\tilde{\Omega} = 50$.

We can write the total number of atoms N of the gas as the sum of the condensed atoms N_0 and the thermal atoms N_T, therefore we have that $N_0 = N - N_T$ where the total number of thermal atoms N_T is obtained by integrating over the space the thermal density $\tilde{n}_T(\tilde{r})$ of Eq.(2.14).

We can compute the critical temperature of condensation $\tilde{T}_c$ for such a gas by using the expression of the total number of atoms N given by Eq.(2.20). By doing so we obtain the critical temperature $T_c = 74$ nK, which in units of the characteristic temperature $T_0 = 4.86 \times 10^{-9}$ K becomes $\tilde{T}_c = 15.32$. As said above at the critical temperature all the atoms are outside the condensate, i.e. $N_0 = 0$, therefore we expect the condensed fraction to be zero at $\tilde{T} = \tilde{T}_c$.

In figure 2.9 a representation of the condensed fraction N_0/N as a function of $\tilde{T}$

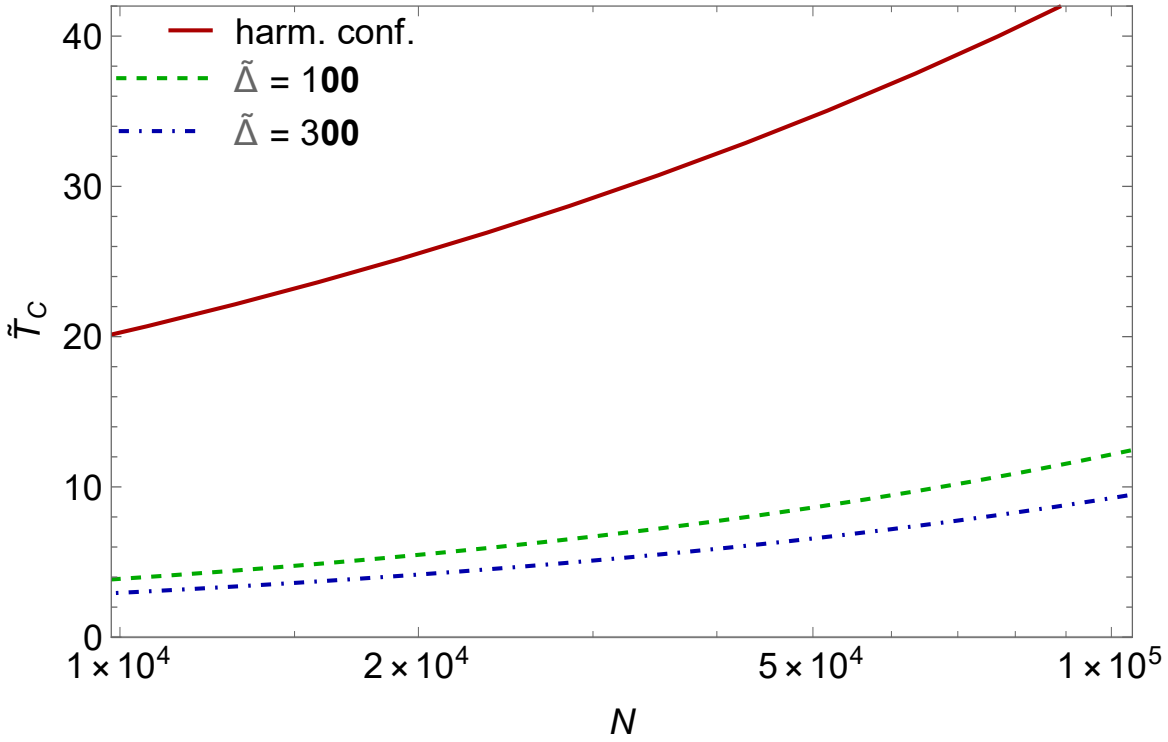

Figure 2.8: Adimensional critical temperature $\tilde{T}_c$ for Bose-Einstein condensation of ^{87}Rb non interacting atoms as a function of the total number of atoms N in the ideal gas. The adimensional critical temperature is compared for different external potential: the adimensional harmonic potential (red line), the adimensional bubble-trap potential of Eq.(1.4) with $\tilde{\Omega} = 50$, $\tilde{\Delta} = 100$ (green dashed line) and $\tilde{\Omega} = 50$, $\tilde{\Delta} = 300$ (blue dot-dashed line). Here the temperatures are expressed in unit of the characteristic temperature $T_0 = 4.860 \times 10^{-9}$ K and the parameters of the external potential $\tilde{\Delta}$ and $\tilde{\Omega}$ are in units of the characteristic energy $E_0 = 6.632 \times 10^{-32}$K. The characteristic quantities are defined in (1.3).

is shown.
As we can see the fraction is equal 1 when the temperature $\tilde{T}$ is zero, indeed all the particles are in the condensate at $\tilde{T} = 0$. Then the value of N_0/N decreases for increasing value of the adimensional temperature $\tilde{T}$ and it goes to zero continuously at the critical temperature $\tilde{T}_c$ as expected.

Notice that to compute the thermal density $\tilde{n}_T(\tilde{r})$ we approximate the chemical potential to the value it assumes at the critical temperature $\tilde{\mu}_c = min_{\tilde{r}}\tilde{U}(\tilde{r})$, then in order to obtain the total number of condensed atoms N_0 we proceeded as described above.

Validity of the semiclassical approximation

The expression of the total density $\tilde{n}(\tilde{r})$ of Eq.(2.15) that we have considered in Eq.(2.19) to compute the total number of atoms N in the gas, is obtained within the

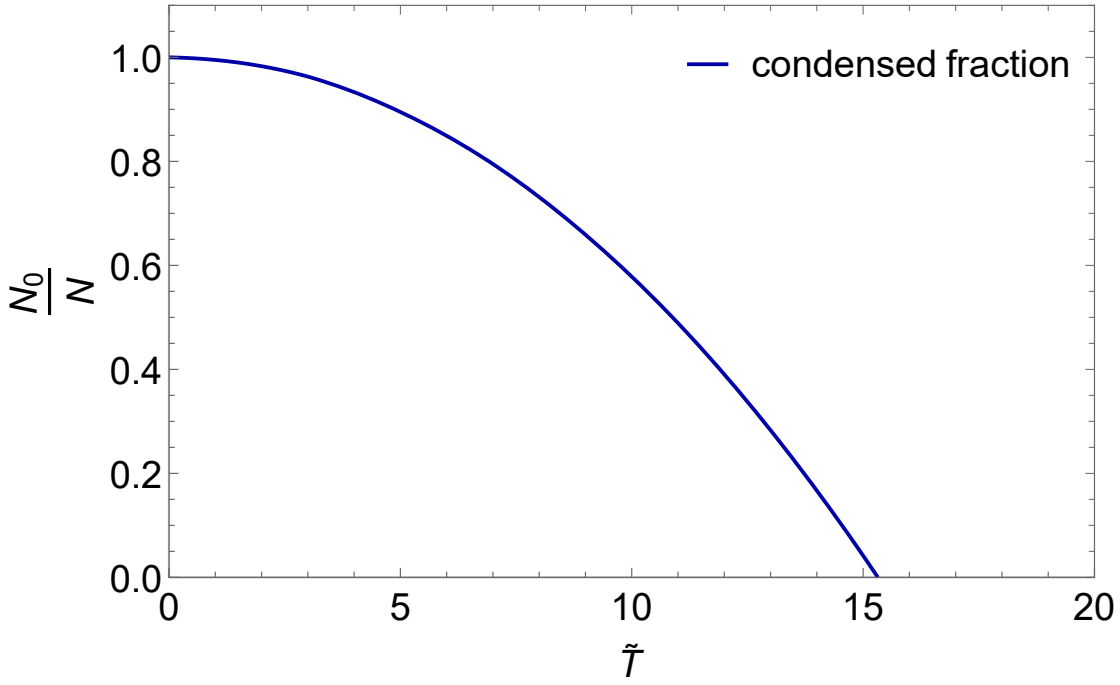

Figure 2.9: Condensed fraction N_0/N as a function of the adimensional temperature $\tilde{T}$ for a system of $N = 1.6 \times 10^5$ non interacting ^{87} Rb atoms in a shell-shaped trap provided by the bubble-trap potential $\tilde{U}(\tilde{r})$ of Eq.(1.4) in which we set the parameters $\tilde{\Delta} = 100$ and $\tilde{\Omega} = 50$. The total number of condensed particles N_0 is computed using $N_0 = N - N_T$ where the total number of thermal particles N_T is obtained by integrating the thermal density $\tilde{n}_T(\tilde{r})$ of Eq.(2.14) over the space. Here the temperature is in unit of $T_0 = 4.860 \times 10^{-9}$ K defined in (1.3).

semiclassical approximation.

The validity of this approximation relies on the inequality

$$k_B T \gg \hbar\omega_k \tag{2.21}$$

where ω_k is the spacing between single-particles levels [24].

In order to estimate ω_k we use the fact that for large values of the parameter Δ, the bubble-trap potential $U(\vec{r})$ of Eq.(1.2) is approximated near its minimum, at $r = r_0$, by a radially shifted harmonic trap [10], namely, by using the scaled unit $\tilde{r} = r/l_0$:

$$U_{rad}(\tilde{r}) = \frac{m}{2}\omega_o^2\, l_o^2\, (\tilde{r} - \tilde{r_0})^2 \tag{2.22}$$

in which m is the atomic mass, the minimum point is $\tilde{r}_0 = 2\sqrt{\tilde{\Delta}}$ and the characteristic length $l_0 = 1.088 \times 10^{-6}$ m is defined in (1.3).

We know that for the harmonic confinement the energy difference between two subsequent levels is constant and given by $\hbar\omega_0$. Moreover, we know that the frequency ω_0 of the harmonic potential $U_{rad}(\tilde{r})$ is linked to the second derivative of

the real potential $U(\tilde{r})$, i.e. the bubble-trap potential of Eq.(1.4), evaluated at its minimum $r = r_0$, namely:

$$m\omega_0^2 = \frac{1}{2}\frac{\partial^2 U(r)}{\partial r^2}\bigg|_{r=r_0} \tag{2.23}$$

which in scaled units becomes:

$$\omega_0 = \omega_c \sqrt{\frac{1}{2}\frac{\partial^2 \tilde{U}(\tilde{r})}{\partial \tilde{r}^2}\bigg|_{\tilde{r}=\tilde{r}_0}} \tag{2.24}$$

where ω_c is the characteristic frequency of the system, that in our case is the frequency of the confinement, $\omega = 2\pi \times 100$ Hz. By computing the derivative we find that $\omega_0 = \sqrt{2\tilde{\Delta}/\tilde{\Omega}}$.

Therefore, if we consider the case in which $\tilde{\Omega} = 50$ and $\tilde{\Delta} = 100$, the accuracy of the semiclassical approximation is expected to be good if the temperature

$$T \gg \frac{\hbar\omega_0}{k_B} \simeq 9nK \tag{2.25}$$

which in units of the characteristic temperature $T_0 = 4.860 \times 10^{-9}$ K defined in (1.3) corresponds to $\tilde{T} \simeq 2$.

Ellipsoidal shell

Let us now consider an ellipsoidal shell, namely a case in which the frequencies of confinement of the harmonic potential $u(\vec{r})$ are now $\vec{\omega} = (100, 100, 30)\, 2\pi$ Hz. The harmonic potential $u(\vec{r})$, introduced in Eq.(1.1), is the one in which the atoms are confined before the radio frequency field is applied to obtained a shell shaped condensate according to the procedure of Zobay and Garraway [15, 16].

Notice that the frequencies along the x and y axes are equal, i.e. $\omega_x = \omega_y = \omega$, therfore we are considering an ellipsoidal shell with an axial symmetry.

The bubble-trap potential for the ellipsoidal shell, has the following expression

$$U(\vec{r}) = 2\sqrt{\left[\frac{m(\omega^2(x^2+y^2)+\omega_z^2 z^2)}{4} - \hbar\Delta\right]^2 + (\hbar\Omega)^2} \tag{2.26}$$

since we are considering an axially symmetric ellipsoidal shell we employ cylindrical coordinates (ρ, z, ϕ) and therefore, since there is no dependency on the angle ϕ, the

potential becomes

$$U(\rho,z)=2\sqrt{\left[\frac{m(\omega^2\rho^2+\omega_z^2z^2)}{4}-\hbar\Delta\right]^2+(\hbar\Omega)^2} \tag{2.27}$$

We want to work with dimensionless units, to do so we employ as the characteristic frequency ω_c of the system the frequency ω of the confinement along the x and y axes. Then we proceed in the same way of the spherical shell, namely we use the characteristic quantities defined in (1.3).

In this way we obtain the following expression for the adimensional bubble-trap potential in cylindrical coordinates

$$\tilde{U}(\tilde{\rho},\tilde{z})=2\sqrt{\left[\frac{1}{4}\left(\tilde{\rho}^2+\left(\frac{\omega_z}{\omega}\right)^2\tilde{z}^2\right)-\tilde{\Delta}\right]^2+\tilde{\Omega}^2} \tag{2.28}$$

a representation of this adimensional potential $\tilde{U}(\tilde{\rho},\tilde{z})$ as a function of $(\tilde{\rho},\tilde{z})$ is shown in Fig.(2.10).

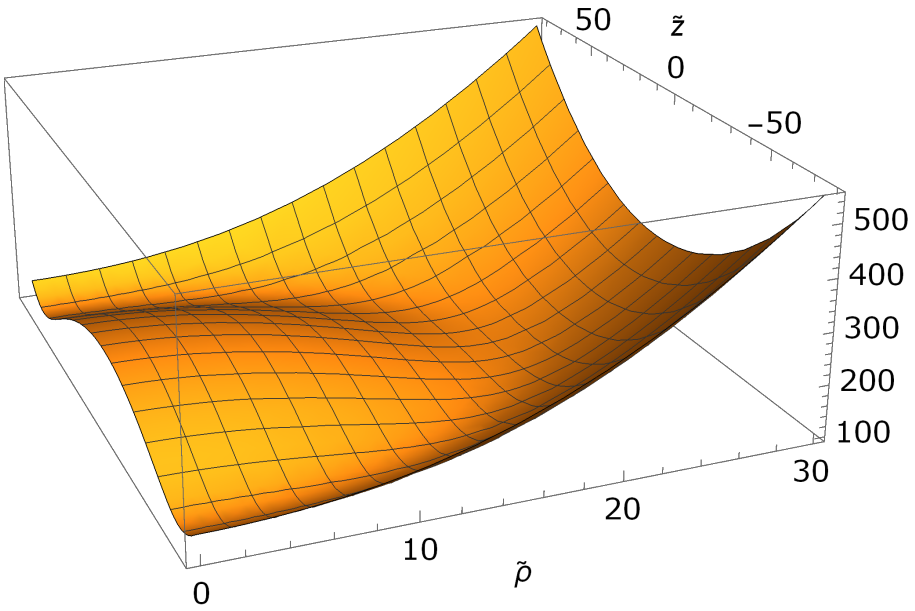

Figure 2.10: Adimensional bubble-trap potential $\tilde{U}(\tilde{\rho},\tilde{z})$ for an ellipsoidal shell as a function of the adimensional length $(\tilde{\rho},\tilde{z})$. The plot is obtained using Eq.(2.28) with the parameter $\tilde{\Omega}=50$ and $\tilde{\Delta}=100$. Here the potential and the parameters are in unit of the characteristic energy $E_o=6.632\times10^{-32}$ J and the coordinates $\tilde{\rho}$ and $\tilde{z}$ are in units of the characteristic length $l_o=1.088\times10^{-6}$ m. The characteristic quantities are defined in (1.3).

Notice that if we set both the parameters of the external potential $\tilde{\Delta}$ and $\tilde{\Omega}$ to zero the adimensional bubble-trap potential $\tilde{U}(\tilde{\rho},\tilde{z})$ of (2.28) reduces to the adimensional ellipsoidal harmonic potential given by

$$\tilde{U}(\tilde{\rho},\tilde{z}) = \frac{1}{2}\left(\tilde{\rho}^2 + \left(\frac{\omega_z}{\omega}\right)^2 \tilde{z}^2\right) \tag{2.29}$$

As done for the spherical shell, we now want to compute the critical temperature $\tilde{T}_c$ of the condensation as a function of the total number of atoms N in the ideal Bose gas. This is obtained by integrating over the space the total density $\tilde{n}(\tilde{\rho},\tilde{z})$ which, within the semiclassical approximation described in section 2.1, is given by

$$\tilde{n}(\tilde{\rho},\tilde{z}) = \left(\frac{\tilde{T}_c}{2\pi}\right) g_{3/2}\left(e^{(2\tilde{\Omega}-\tilde{U}(\tilde{\rho},\tilde{z}))/\tilde{T}_c}\right) \tag{2.30}$$

where we used the fact that at the critical temperature of condensation $\tilde{T}_c$ the adimensional chemical potential $\tilde{\mu}_c$ is equal to the minimum of the external potential $\tilde{U}(\tilde{\rho},\tilde{z})$, namely $\tilde{\mu}_c = min_{\tilde{\rho},\tilde{z}}\,\tilde{U}(\tilde{\rho},\tilde{z}) = 2\tilde{\Omega}$.

The total number of atoms N in the gas which such to have as the critical temperature $\tilde{T}_c$ the one we are considering is therefore is given by

$$N = 2\pi \int_{-\infty}^{\infty} d\tilde{z} \int_0^{\infty} d\tilde{\rho}\,\tilde{\rho}\left(\frac{\tilde{T}_c}{2\pi}\right)^{\frac{3}{2}} g_{\frac{3}{2}}\left(e^{\frac{2}{\tilde{T}_c}(\tilde{\Omega}-\sqrt{[\frac{1}{4}(\tilde{\rho}^2+(\frac{\omega_z}{\omega})^2\tilde{z}^2)-\tilde{\Delta}]^2-\tilde{\Omega}^2}}\right) \tag{2.31}$$

where due to the axial symmetry the integral over the angle ϕ simply is 2π.

The integrals defining the total number of atoms N in the gas in Eq.(2.31) have to be solved numerically. We do so for different values of the critical temperature T_c, then we proceed in the same way we did for the spherical shell by plotting the various critical temperatures T_c that we have considered on the y-axis and the corresponding total number of atoms N in the gas that we have obtained from the integration in the x-axis.

In this way we obtain a representation of the critical temperature of condensation $\tilde{T}_c$ as a function of the total number of atoms N in the Bose gas which is shown in Fig. 2.11.

As done in the case of the spherical shell we consider as the external potential $\tilde{U}(\tilde{r})$ confining the gas the adimensional bubble-trap potential of Eq.(2.28) in which we set $\tilde{\Omega} = 50$, $\tilde{\Delta} = 100$ (pink line) and $\tilde{\Omega} = 50$, $\tilde{\Delta} = 300$ (dot-dashed blue line) which respectively provides a thicker shell with a smaller size and to a thinner shell with a larger size.

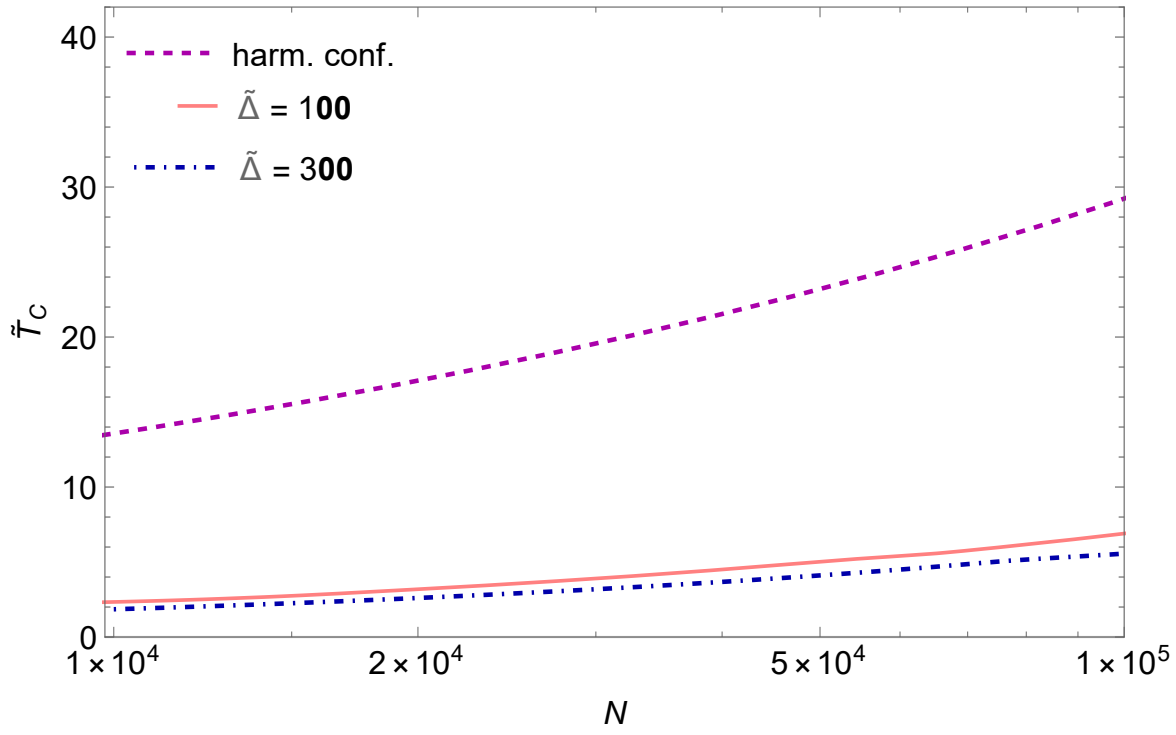

Figure 2.11: Adimensional critical temperature $\tilde{T}_c$ for Bose-Einstein condensation of ^{87}Rb non interacting atoms as a function of the total number of atoms N. The adimensional critical temperature is compared for different external potential: the adimensional ellipsoidal harmonic trap (dashed violet line) given by Eq.(2.29), the adimensional ellipsoidal bubble-trap potential of Eq.(2.28) with $\tilde{\Omega} = 50$, $\tilde{\Delta} = 100$ (pink line) and $\tilde{\Omega} = 50$, $\tilde{\Delta} = 300$ (blue dot-dashed line). Here the temperatures are expressed in unit of the characteristic temperature $T_o = 4.860 \times 10^{-9}$ K and the parameters of the external potential $\tilde{\Delta}$ and $\tilde{\Omega}$ are in units of the characteristic energy $E_0 = 6.632 \times 10^{-32}$K. The characteristic quantities are defined in (1.3).

Finally, for comparison we also consider an ideal Bose gas in an harmonic ellipsoidal confinement (dashed magenta line) described by the adimensional potential of Eq.(2.29). Notice that the harmonic ellipsoidal potential is the potential to which the bubble-trap potential $\tilde{U}(\tilde{\rho}, \tilde{z})$ of Eq.(2.28) reduces if both the parameters are zero $\tilde{\Delta} = \tilde{\Omega} = 0$.

As we can see from figure 2.11 we found results similar to the ones found for the spherical shell shown in Fig. 2.8, namely we have that, for a fixed value of the total number N of atoms in the gas, the critical temperature $\tilde{T}_c$ of condensation is slightly lower when the gas is trapped by the bubble -trap potential having the detuning $\tilde{\Delta} = 300$ which provides a thinner shell with a larger size, than the one for the gas trapped by the bubble-trap potential with $\tilde{\Delta} = 100$ which provides a thicker shell with a small size.

Moreover, for a fixed number of atoms N the critical temperature of condensation $\tilde{T}_c$ is much bigger when the gas is in a conventional trap, provided by the harmonic potential $\tilde{U}(\tilde{\rho}, \tilde{z})$ of Eq.(2.29), with respect to the critical temperature for the gas in

a shell-shaped trap, provided by the bubble-trap potential of Eq.(2.28), both for the thinner and the thicker shell-shaped trap.

As described above we have found that in the ellipsoidal case the critical temperatures of condensation $\tilde{T}_c$ for an ideal Bose gas in the different trapping configuration that we have considered, i.e. the full filled geometry and the hollow one for the two shell with different dimension and thickness, relate to one another in a similar way of the ones for the case of a spherical shell.

In Fig. 2.12 we show a comparison between the results obtained by employing as the external potential confining the atoms the harmonic potential and the bubble-trap potential $\tilde{U}(\tilde{r})$ in which we set the parameters $\tilde{\Delta} = 100$ and $\tilde{\Omega} = 50$.

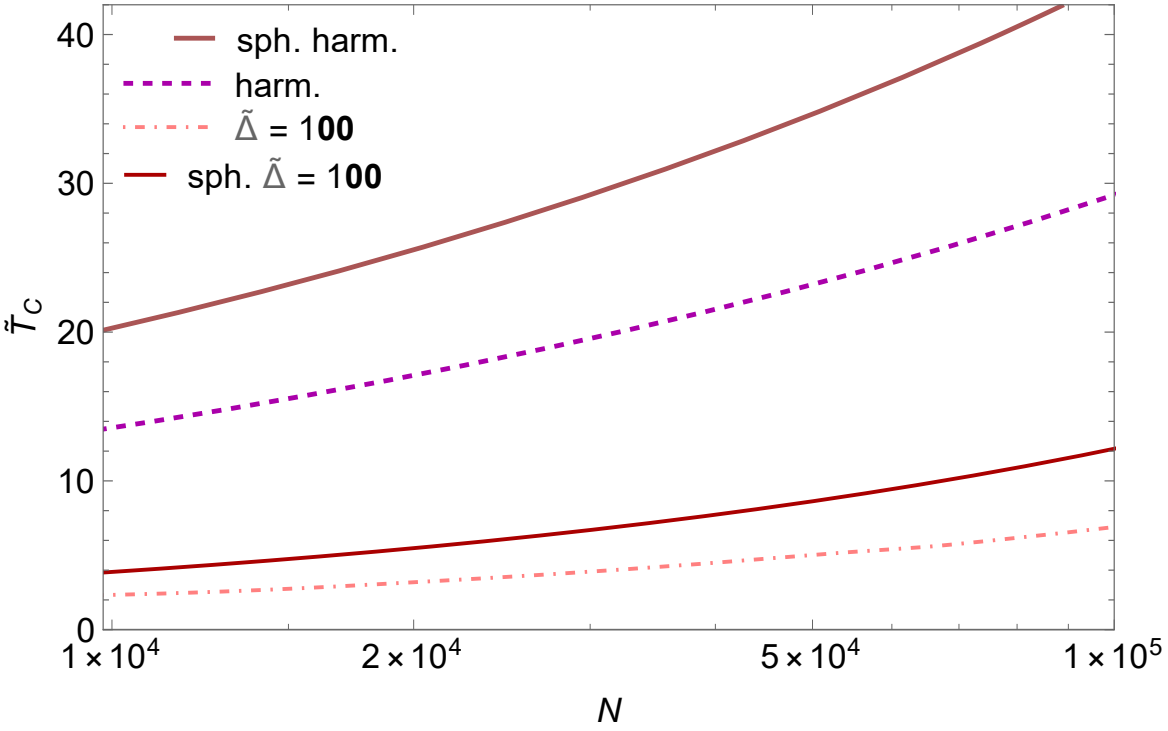

Figure 2.12: Adimensional critical temperature $\tilde{T}_c$ for Bose-Einstein condensation of ^{87}Rb non interacting atoms as a function of the total number of atoms N. The adimensional critical temperature is compared for different external potential: the adimensional spherical harmonic potential (dark pink line) given by (2.29), the adimensional ellipsoidal harmonic trap (dashed violet line) given by Eq.(2.29), the adimensional spherical bubble-trap potential (red line) of Eq.(2.28) with $\tilde{\Omega} = 50$, $\tilde{\Delta} = 100$ and the adimensional ellipsoidal bubble-trap potential (dot-dashed pink line) given by Eq.(2.29) with $\tilde{\Omega} = 50$, $\tilde{\Delta} = 100$. Here the temperatures are expressed in unit of the characteristic temperature $T_o = 4.860 \times 10^{-9}$ K and the parameters of the external potential $\tilde{\Delta}$ and $\tilde{\Omega}$ are in units of the characteristic energy $E_0 = 6.632 \times 10^{-32}$K. The characteristic quantities are defined in (1.3).

In particular we consider the case of a spherical shell for which the bubble-trap

potential (red line) is given by Eq.(1.4) and the harmonic one (dark brown line) is given by Eq.(1.5) and an axially symmetric ellipsoidal shell for which the bubble-trap potential (dot-dashed pink line) is given by Eq.(2.28) and the harmonic one (dashed magenta line) by Eq.(2.29).

As we can see from the figure 2.12 for a fixed number of atoms N in the ideal gas the quantum degeneracy is harder to reach when the gas is trapped in the ellipsoidal shell (dashed lines), indeed in this trapping configuration the critical temperature is smaller than the one obtained for the gas trapped in the spherical shell (continuous line). This behaviour is also shown, and it is in particular more evident, for the full filled geometry obtained by employing as the external potential the harmonic potential.

Chapter 3

Thermodynamics of a shell-shaped interacting gas

In this chapter we study a dilute gas of strongly interacting bosons in a shell-shaped trap.We start by introducing the formalism to described such a system, in particular we derive the Popov equations and the spectrum of the excitations using the semiclassical approximation. We then proceed by treating the interaction in the Hartree-Fock approximation, in which the thermal atoms are assumed to behave as a non interacting gas in a self-consistent mean-filed, and within this approximation we calculate the critical temperature of condensation for the trapped interacting gas by employing an iterative procedure to compute the density. The results are then compared with the ones for the ideal gas.

Afterwards we compute the thermal density and the condensate one at temperature lower than the critical one for a gas in a shell-shaped trap and a representation of the density profiles as a function of the radius is given.
Finally, we compute and represent the condensate and thermal fraction as a function of the temperature and we compare it to the results obtained for the ideal gas.

3.1 Interacting Bose gas

Let us now proceed by considering a dilute gas of interacting bosons.
The dimensionless parameter controlling the validity of this approximation [20] is the number of particles in a "scattering volume" a_s^3, this can be written as $\bar{n}a_s^3$, where a_s is the s-wave scattering length and $\bar{n}$ is the average density of the gas.

For the system of ^{87}Rb atoms that we are considering the scattering length is $a_{s,Rb} = 50\dot{A}$ (Boesten et al., 1997), meaning the interaction is repulsive since $a_{s,Rb}$ is positive. The system is said to be dilute when $\bar{n}a_s^3 \gg 1$.

In a dilute and cold gas [23], only binary collisions at low energy are relevant and these collisions are characterized by a single parameter, the s-wave scattering length a_s, independently of the details of the two-body potential. Therefore the effective low-energy interaction $V(\vec{r}_1 - \vec{r}_2)$ between two atoms at $\vec{r}_1$ and $\vec{r}_2$ can be approximated as a contact interaction

$$V(\vec{r}_1 - \vec{r}_2) = \frac{4\pi\hbar^2 a_s}{m}\delta(\vec{r}_1 - \vec{r}_2) \tag{3.1}$$

let us define

$$g = \frac{4\pi\hbar^2 a_s}{m} \tag{3.2}$$

as the coupling constant.

A gas of identical atoms is described by a bosonic field operator $\hat{\Psi}(\vec{r}, t)$. In the grand canonical ensamble the system is described by an effective Hamiltonian $\hat{K} = \hat{H} - \mu\hat{N}$, therefore the equation of motion for the field operator at finite temperature is given by [27]

$$i\hbar\frac{\partial\hat{\Psi}(\vec{r}, t)}{\partial t} = \left[-\frac{\hbar^2}{2m}\nabla^2 + U(\vec{r}) - \mu + g\hat{\Psi}^+(\vec{r}, t)\hat{\Psi}(\vec{r}, t)\right]\hat{\Psi}(\vec{r}, t) \tag{3.3}$$

where we used the fact that for a dilute gas the interatomic potential can be approximated as a contact interaction $V(\vec{r}_1 - \vec{r}_2) = g\delta^3(\vec{r}_1 - \vec{r}_2)$ with g the coupling constant of Eq.(3.2).

In the bosonic field operator $\hat{\Psi}(\vec{r}, t)$ one can separate out the Bose condensed particles from the non-condensed ones by using the following Bogoliubov prescription [28]

$$\hat{\Psi}(\vec{r}, t) = \Phi(\vec{r}) + \hat{\phi}(\vec{r}, t) \tag{3.4}$$

where $\Phi(\vec{r})$ is the order parameter (macroscopic wavefunction) of the condensate defined as the mean value in the grand-canonical ensamble of the field operator, i.e. $\Phi(\vec{r}) = \langle\hat{\Psi}(\vec{r}, t)\rangle$, and $\hat{\phi}(\vec{r}, t)$ is the fluctuation operator which describes the non-condensed fraction of the atoms.

The Bogoliubov prescription enables us to write the three-body thermal average in the following way [29]

$$\langle\hat{\Psi}^+(\vec{r})\hat{\Psi}(\vec{r})\hat{\Psi}(\vec{r})\rangle = |\Phi(\vec{r}, t)|^2\Phi(\vec{r}, t) + 2\Phi(\vec{r})\langle\hat{\phi}^+(\vec{r}, t)\hat{\phi}(\vec{r}, t)\rangle + \Phi(\vec{r})^*\langle\hat{\phi}(\vec{r}, t)\hat{\phi}(\vec{r}, t)\rangle \tag{3.5}$$

where we have consider the self-consistent mean-field approximation, namely

$$\hat{\phi}^+(\vec{r}, t)\hat{\phi}(\vec{r}, t)\hat{\phi}(\vec{r}, t) \simeq 2\langle\hat{\phi}^+(\vec{r}, t)\hat{\phi}(\vec{r}, t)\rangle\hat{\phi}(\vec{r}, t) + \langle\hat{\phi}(\vec{r}, t)\hat{\phi}(\vec{r}, t)\rangle\hat{\phi}^+(\vec{r}, t) \tag{3.6}$$

We obtain an equation for the order parameter $\Phi(\vec{r})$ by taking the average of the equation of motion (3.3), in this way we find

$$\left(-\frac{\hbar^2}{2m}\nabla^2 + U(\vec{r}) - \mu \right)\Phi(\vec{r}) + g[n_0(\vec{r}) + 2\tilde{n}(\vec{r})]\Phi(\vec{r}) + g\tilde{m}(\vec{r})\Phi^*(\vec{r}) = 0 \qquad (3.7)$$

where we have introduced the following local densities

$$\begin{aligned} n_0(\vec{r}) &\equiv |\Phi(\vec{r})|^2, \\ \tilde{n}(\vec{r}) &\equiv \langle \hat{\phi}^+(\vec{r},t)\hat{\phi}(\vec{r},t)\rangle, \\ \tilde{m}(\vec{r}) &\equiv \langle \hat{\phi}(\vec{r},t)\hat{\phi}(\vec{r},t)\rangle \end{aligned} \qquad (3.8)$$

which respectively are the condensate density $n_0(\vec{r})$, the non-condensed density $\tilde{n}(\vec{r})$ and the anomalous non-condensate density $\tilde{m}(\vec{r})$.

Note that if all the particles are in the condensate, i.e. $\tilde{n}(\vec{r}) = \tilde{m}(\vec{r}) = 0$, called the Bogoliubov approximation, the equation of motion (3.7) reduces to the Gross-Pitaevskii equation [29, 30], which is appropriate only at $T \simeq 0$.

Another possible less drastic approximation is the Popov approximation [31] in which we keep $\tilde{n}(\vec{r})$ but neglect the anomalous density $\tilde{m}(\vec{r})$ as being small compared to $n_0(\vec{r})$ and $\tilde{n}(\vec{r})$.
In this case the equation of motion for the order parameter becomes the so-called finite-temperature Gross-Pitaevskii equation

$$\left[-\frac{\hbar^2}{2m}\nabla^2 + U(\vec{r}) + gn_0(\vec{r}) + 2g\tilde{n}(\vec{r}) \right]\Phi(\vec{r}) = \mu\Phi(\vec{r}) \qquad (3.9)$$

which is not closed, hence we must add an equation for the non-condensed density $\tilde{n}(\vec{r})$ which is found by studying the fluctuations operator $\hat{\phi}(\vec{r},t)$.
Note that the Popov approximation reduces to the Bogoliubov approximation at $T \simeq 0$ where also $\tilde{n}(\tilde{r})$ becomes negligible.

The equation for the fluctuation operator $\hat{\phi}(\vec{r},t)$ is obtained by subtracting from the equation of motion Eq.(3.3) for the field operator $\hat{\Psi}(\vec{r},t)$ its average, which gave us the equation for the order parameter $\Phi(\vec{r})$, namely

$$i\hbar\frac{\partial\hat{\phi}(\vec{r},t)}{\partial t} = \left[-\frac{\hbar^2}{2m}\nabla^2 + U(\vec{r}) - \mu \right]\hat{\phi}(\vec{r},t) + g[\hat{\Psi}^+(\vec{r},t)\hat{\Psi}(\vec{r},t)\hat{\Psi}(\vec{r},t) - \langle \hat{\Psi}^+(\vec{r})\hat{\Psi}(\vec{r})\hat{\Psi}(\vec{r})\rangle] \qquad (3.10)$$

To find the thermal excitations above the condensate one can simply linearize the previous equation [29, 33]. This can be done by means of the mean-field approximation, namely. we use

$$\begin{aligned}\hat{\phi}^+(\vec{r},t)\hat{\phi}(\vec{r},t) &\simeq \langle\hat{\phi}^+(\vec{r},t)\hat{\phi}(\vec{r},t)\rangle = \tilde{n}(\vec{r}) \\ \hat{\phi}(\vec{r},t)\hat{\phi}(\vec{r},t) &\simeq \langle\hat{\phi}(\vec{r},t)\hat{\phi}(\vec{r},t)\rangle = \tilde{m}(\vec{r})\end{aligned} \tag{3.11}$$

The linearized motion equation for the fluctuations operator (3.10) reduces to

$$i\hbar\frac{\partial\hat{\phi}(\vec{r},t)}{\partial t} = \Big[-\frac{\hbar^2}{2m}\nabla^2 + U(\vec{r}) - \mu\Big]\hat{\phi}(\vec{r},t) + 2gn(\vec{r})\hat{\phi}(\vec{r},t) + g[\Phi^2(\vec{r}) + \tilde{m}(\vec{r})]\hat{\phi}^+(\vec{r},t) \tag{3.12}$$

where $n(\vec{r}) = n_0(\vec{r}) + \tilde{n}(\vec{r})$ is the total density.

The analogous equation for $\hat{\phi}^+(\vec{r},t)$ can be easily derived following the same procedure. The coupled equations of motions given by (3.7) and (3.12) correspond to the Hartree-Fock-Bogoliubov (HFB) approximation.

Due to the presence of the self-adjoint operator $\hat{\phi}^+(\vec{r},t)$ in Eq.(3.12), the fluctuations operator must be expanded using the Bogoliubov linear transformation [33]

$$\hat{\phi}(\vec{r},t) = \sum_j \Big[u_j(\vec{r})e^{-iE_jt/\hbar}\hat{a}_j + v_j^*(\vec{r})e^{iE_jt/\hbar}\hat{a}_j^+\Big] \tag{3.13}$$

where $\hat{a}_j$ and $\hat{a}_j^+$ are annihilation and creation operators satisfying the usual Bose commutation relations and the complex functions $u_j(\vec{r})$ and $v_j(\vec{r})$ are the wavefunctions of the so-called quasi-particles excitations of energy E_j. These functions satisfy the normalization condition

$$\int d^3\vec{r}[u_j^*(\vec{r})u_k(\vec{r}) - v_j^*(\vec{r})v_k(\vec{r})] = \delta_{jk} \tag{3.14}$$

By inserting the expansion of the fluctuation operator (3.13) into the equation of motion (3.12) within the Popov approximation, i.e. $m(\vec{r}) = 0$, we obtain two eigenvalue equations for the excitations, the so-called Popov equations

$$\begin{aligned}\Big[-\frac{\hbar^2\nabla^2}{2m}+U(\vec{r})-\mu+2gn(\vec{r})\Big]u_j(\vec{r})+g\Phi^2(\vec{r})v_j(\vec{r})=E_j(\vec{r})u_j(\vec{r})\\ \Big[-\frac{\hbar^2\nabla^2}{2m}+U(\vec{r})-\mu+2gn(\vec{r})\Big]v_j(\vec{r})+g\Phi^2(\vec{r})u_j(\vec{r})=-E_j(\vec{r})v_j(\vec{r})\end{aligned} \tag{3.15}$$

where $n(\vec{r})$ is the total density and E_j is the energy of the elementary excitations of the system.

Equations (3.7) and (3.15) are supplemented by the condition fixing the total number of atoms in the system [33]

$$N=\int d^3\vec{r}[n_0(\vec{r})+\tilde{n}(\vec{r})] \tag{3.16}$$

where $n_0(\vec{r})=|\Phi(\vec{r})|^2$ is the condensed density and $\tilde{n}(\vec{r})$ is the non-condensed density which, using (3.13), is

$$\tilde{n}(\vec{r})=\sum_j(|u_j(\vec{r})|^2+|v_j(\vec{r})|^2)\langle\hat{a}_j^+\hat{a}_j\rangle+|v_j(\vec{r})|^2 \tag{3.17}$$

where $\langle\hat{a}_j^+\hat{a}_j\rangle$ is the Bose distribution for the quasiparticles excitations

$$\langle\hat{a}_j^+\hat{a}_j\rangle=\frac{1}{e^{E_j/k_BT}-1} \tag{3.18}$$

Note that also at zero temperature there is a non-condensed density, the quantum depletion given by $\sum_j|v_j(\vec{r})|^2$, the other contribution is the thermal density $n_T(\vec{r})$.

The coupled equations (3.15) can be easily solved if one consider the semiclassical approximation which gives reliable results, as we have seen in Eq.(2.21), only if $k_BT\gg\hbar\omega_j$, namely if the temperature is much larger than the spacing between single-particles levels [20, 24].

We write

$$u_j(\vec{r})=u(\vec{r},\vec{p})e^{i\varphi(\vec{r})}\qquad v_j(\vec{r})=v(\vec{r},\vec{p})e^{i\varphi(\vec{r})} \tag{3.19}$$

where $\vec{p}=\hbar\nabla\varphi$ is fixed by the gradient of the phase, moreover we assume that $u_j(\vec{r})$ and $v_j(\vec{r})$ are smooth functions of $\vec{r}$.

In this approximation the sum over states j is replaced by the integral $\int d^3\vec{p}/(2\pi\hbar)^3$ and by neglecting derivatives of u and v and the second derivatives of φ we can rewrite the Popov equations (3.15) in the semiclassical form

$$\begin{aligned}\left(\frac{p^2}{2m}+U(\vec{r})-\mu+2gn(\vec{r})\right)u(\vec{r},\vec{p})+g\Phi^2(\vec{r})v(\vec{r},\vec{p})=E(\vec{r},\vec{p})u(\vec{r},\vec{p})\\ \left(\frac{p^2}{2m}+U(\vec{r})-\mu+2gn(\vec{r})\right)v(\vec{r},\vec{p})+g\Phi^2(\vec{r})u(\vec{r},\vec{p})=-E(\vec{r},\vec{p})v(\vec{r},\vec{p})\end{aligned} \tag{3.20}$$

from these one finds the following spectrum of elementary excitations [20]

$$E(\vec{r},\vec{p})=\left(\left(\frac{p^2}{2m}+U(\vec{r})-\mu+2gn(\vec{r})\right)^2-g^2n_0^2(\vec{r})\right)^{1/2} \tag{3.21}$$

Neglecting the amplitudes $v_j(\vec{r})$, i.e. $v_j(\vec{r})=0$, or better the coupling between $u_j(\vec{r})$ and $v_j(\vec{r})$, we have the Hartree-Fock approximation [21,34] in which the Popov equations (3.15) reduces to

$$\left[-\frac{\hbar^2\nabla^2}{2m}+U(\vec{r})-\mu+2gn(\vec{r})\right]u_j(\vec{r})=E_j(\vec{r})u_j(\vec{r}) \tag{3.22}$$

and the non-condensed particles $\tilde{n}(\vec{r})$ coincides with the thermal particles $n_T(\vec{r})$ because the quantum depletion is zero, i.e. we are neglecting it.

In this approximation the quasi-particles, i.e. the thermal particles, behave as non interacting Bosons moving in the effective potential

$$U_{eff}=U(\vec{r})+2gn(\vec{r}) \tag{3.23}$$

and in the semiclassical approximation one finds the following spectrum of excitations

$$E(\vec{r},\vec{p})=\frac{p^2}{2m}+U(\vec{r})-\mu+2gn(\vec{r}) \tag{3.24}$$

the so-called Hartree-Fock spectrum, and the thermal density is given by

$$n_T(\vec{r})=\int\frac{d^3\vec{p}}{(2\pi\hbar)^3}\frac{1}{e^{E(\vec{r},\vec{p})/k_BT}-1} \tag{3.25}$$

which integrated gives

$$n_T(\vec{r})=\frac{1}{\lambda_T^3}g_{3/2}\left(e^{(\mu-U(\vec{r})-2gn(\vec{r}))/k_BT}\right)=\frac{1}{\lambda_T^3}g_{3/2}\left(e^{(\mu-U_{eff}(\vec{r}))/k_BT}\right) \tag{3.26}$$

notice that this is the ideal gas formula for the thermal density in which the external potential $U(\vec{r})$ is replaced by the effective potential $U_{eff}(\vec{r})$ defined in Eq.(3.23).

Finally the chemical potential is fixed by the normalization condition

$$N = \int d^3\vec{r}\ [n_0(\vec{r}) + n_T(\vec{r})] \tag{3.27}$$

3.2 Critical temperature for an interacting Bose gas

We proceed by considering an interacting gas of ^{87}Rb atoms trapped by an external potential $U_{ext}(\vec{r})$. We treat the interaction in the mean-field approximation by considering the Hartree-Fock theory [23]. As said above, in this model we assume the thermal atoms to behave as non interacting bosons in a self-consistent mean field.

The single particle Hamiltonian is given by

$$H_{HF} = -\frac{\hbar^2\nabla^2}{2m} + U_{eff}(\vec{r}) \tag{3.28}$$

where the effective potential $U_{eff}(\vec{r}) = U_{ext}(\vec{r}) + U_{MF}(\vec{r})$ is defined in Eq.(3.23) in which the last term

$$U_{MF}(\vec{r}) = 2gn(\vec{r}) \tag{3.29}$$

is a mean field generated by interactions with other atoms, with $g = 4\pi\hbar^2 a_s/m$ the coupling constant. The quantity $n(\vec{r})$ is the total density of the system, given by the sum of both the condensate $n_0(\vec{r})$ and the thermal component $n_T(\vec{r})$.

Notice that as pointed out in the previous section in the Hartree-Fock approximation we are neglecting the quantum depletion at $T = 0$.

At the critical temperature of condensation $T = T_c$, since there are no atoms in the condensate, i.e. $N_0 = 0$, the total density $n(\vec{r})$ is equal to the thermal density $n_T(\vec{r})$ of Eq.(3.32), namely it is given by

$$n(\vec{r}) = \frac{1}{\lambda^3_{T_c}} g_{\frac{3}{2}}\left(e^{(\mu_c - U_{eff}(\vec{r}))/k_B T_c}\right) \tag{3.30}$$

where the chemical potential at the critical temperature T_c is now equal to the minimum of the effective potential $U_{eff}(\vec{r})$, namely $\mu_c = min_r\, U_{eff}(\vec{r}) = min_r(U_{ext}(\vec{r}) +$

$2gn(\vec{r})$).

Let us now use adimensional quantities: the critical chemical potential $\tilde{\mu}_c$ in unit of the characteristic energy $E_0 = 6.632 \times 10^{-32} J$ defined in (1.3) becomes

$$\tilde{\mu}_c = min_{\tilde{r}}\, \tilde{U}_{eff}(\tilde{r}) = min_{\tilde{r}}(\tilde{U}_{ext}(\tilde{r}) + 2\tilde{g}\tilde{n}(\tilde{r})) \tag{3.31}$$

where the adimensional coupling constant is $\tilde{g} = 4\pi\tilde{a}_s$ with the adimensional scattering length $\tilde{a}_s = a_s/l_0 = 4.6 \times 10^{-3}$.

The adimensional total density, at the critical temperatures $\tilde{T} = \tilde{T}_c$, becomes

$$\tilde{n}(\tilde{r}) = \left(\frac{\tilde{T}_c}{2\pi}\right)^{\frac{3}{2}} g_{\frac{3}{2}}\left(e^{(\tilde{\mu}_c - \tilde{U}(\tilde{r}) - 2\tilde{g}\tilde{n}(\tilde{r}))/\tilde{T}_c}\right) = \left(\frac{\tilde{T}_c}{2\pi}\right)^{\frac{3}{2}} g_{\frac{3}{2}}\left(e^{(\tilde{\mu}_c - \tilde{U}_{eff}(\tilde{r}))/\tilde{T}_c}\right) \tag{3.32}$$

with the critical temperature in units of the characteristic temperature $T_0 = 4.860 \times 10^{-9}$ J and the total density in units of l_0^3 with $l_0 = 1.088 \times 10^{-6}$ m as described in (1.3).

As done for the ideal Bose gas we now want to compute the critical temperature of condensation T_c for the trapped interacting Bose gas as a function of the total number of atoms N in the gas.

We proceed in the same way of the ideal gas, namely we fix a value for the critical temperature T_c and we compute the total number of atoms N of the interacting gas, which is such to have that critical temperature T_c, by integrating over the space the total density $\tilde{n}(\tilde{r})$ given by Eq.(3.32).

The expression (3.32) of the total density $\tilde{n}(\tilde{r})$ has to be solved in a self-consistent way since the total density $\tilde{n}(\tilde{r})$ also appears in the mean-field potential $\tilde{U}_{MF}(\vec{r}) = 2\tilde{g}\tilde{n}(\tilde{r})$ on the right hand side of the equation.

To do so we employ an iterative procedure in which we begin by considering as the mean-field potential $\tilde{U}_{MF}(\vec{r})$ on the right hand side of the expression for the total density $\tilde{n}(\tilde{r})$ of Eq.(3.32) the potential obtained by using as the total density the one of the ideal non interacting gas $n^{(0)}(\vec{r})$ that we have already computed in the previous chapter, namely

$$\tilde{n}^{(0)}(\tilde{r}) = \left(\frac{\tilde{T}_c}{2\pi}\right)^{\frac{3}{2}} g_{\frac{3}{2}}\left(e^{\frac{1}{\tilde{T}_c}(2\tilde{\Omega} - \tilde{U}(\tilde{r}))}\right) \tag{3.33}$$

where we used the fact that the critical chemical potential is equal the minimum of the external potential, i.e. $\tilde{\mu}_c^{(0)} = min_{\tilde{r}}\, \tilde{U}(\tilde{r}) = 2\tilde{\Omega}$.

Notice that we used the label $^{(0)}$ to indicate that this is the order zero of the iterative procedure.

Therefore the mean-field potential at this order is given by $\tilde{U}^{(0)}_{MF}(\tilde{r}) = 2\tilde{g}\tilde{n}^{(0)}(\tilde{r})$.

At this point, for a fixed value of the critical temperature T_c we can compute the chemical potential $\tilde{\mu}^{(1)}_c$ at the first order, which is equal to the minimum of the effective potential at this order which is given by

$$\tilde{U}^{(1)}_{eff}(\tilde{r}) = \tilde{U}(\tilde{r}) + \tilde{U}^{(0)}_{MF}(\tilde{r}) \tag{3.34}$$

therefore the chemical potential is

$$\tilde{\mu}^{(1)}_c = min_{\tilde{r}} \left(\tilde{U}(\tilde{r}) + \tilde{U}^{(0)}_{MF}(\tilde{r})\right) \tag{3.35}$$

hence the total density at the first order is given by

$$\tilde{n}^{(1)}(\tilde{r}) = \left(\frac{\tilde{T}_c}{2\pi}\right)^{\frac{3}{2}} g_{\frac{3}{2}}\left(e^{(\tilde{\mu}^{(1)}_c - \tilde{U}(\tilde{r}) - \tilde{U}^{(0)}_{MF}(\tilde{r}))/\tilde{T}_c}\right) \tag{3.36}$$

Then we proceed by computing the total density at the next order, to do so we consider as the mean field $\tilde{U}^{(1)}_{MF}(\tilde{r}) = 2\tilde{g}\tilde{n}^{(1)}(\tilde{r})$ and the procedure described above is then repeated until convergence is reached, namely until in the following expression for the density at the i-th order

$$\tilde{n}^{(i)}(\tilde{r}) = \left(\frac{\tilde{T}_c}{2\pi}\right)^{\frac{3}{2}} g_{\frac{3}{2}}\left(e^{(\tilde{\mu}^{(i)}_c - \tilde{U}(\tilde{r}) - 2g\tilde{n}^{(i-1)}(\tilde{r})(\tilde{r}))/\tilde{T}_c}\right) \tag{3.37}$$

the total densities $\tilde{n}(\tilde{r})$ in the in the two side of the equation are equal.

Once we have obtained the expression for the total density $\tilde{n}(\tilde{r})$ by using the procedure just described we want to compute the critical temperature of condensation T_c as a function of the total number of atoms N in the gas.

As described above, once we fixed a value for the critical temperature $\tilde{T}_c$, in order to obtain the total number of atoms N in the gas at that critical temperature T_c, i.e. the total number of atoms N in the interacting gas which is such to have as the critical temperature of condensation $\tilde{T}_c$ the one that we are considering, we integrate over the space the expression of the total density $\tilde{n}(\tilde{r})$ given by Eq.(3.32) that we have just computed.

By employing spherical coordinates the total number of atoms N is given by

$$N = 4\pi \int_0^\infty d\tilde{r}\ \tilde{r}^2 \left(\frac{\tilde{T}_c}{2\pi}\right)^{\frac{3}{2}} g_{\frac{3}{2}}\left(e^{\ \frac{1}{\tilde{T}_c}(\tilde{\mu}_c - \tilde{U}(\tilde{r}) - \tilde{U}_{MF}(\tilde{r}))}\right) \tag{3.38}$$

in order to obtain a representation of the critical temperature of condensation as a function of the total number of atoms N in the gas the iterative procedure illustrated

above to compute the total density $\tilde{n}(\tilde{r})$ at a fixed critical temperature $\tilde{T}_c$ has to be repeated for different values of the critical temperature $\tilde{T}_c$ and then we proceed by integrating it over the space, similarly to what we did in the case of a non interacting gas.

In Fig. 3.1 we plot the critical temperature of condensation $\tilde{T}_c$ as a function of the total number of atoms N in the gas. We show a comparison of the results obtained by considering different trapping configuration, namely different external potential: the harmonic confinement of Eq.(1.5) (dot-dashed blue line), the bubble-trap potential of Eq.(1.4) with $\tilde{\Omega} = 50$, $\tilde{\Delta} = 100$ (violet line) and $\tilde{\Omega} = 50$, $\tilde{\Delta} = 300$ (dashed green line).

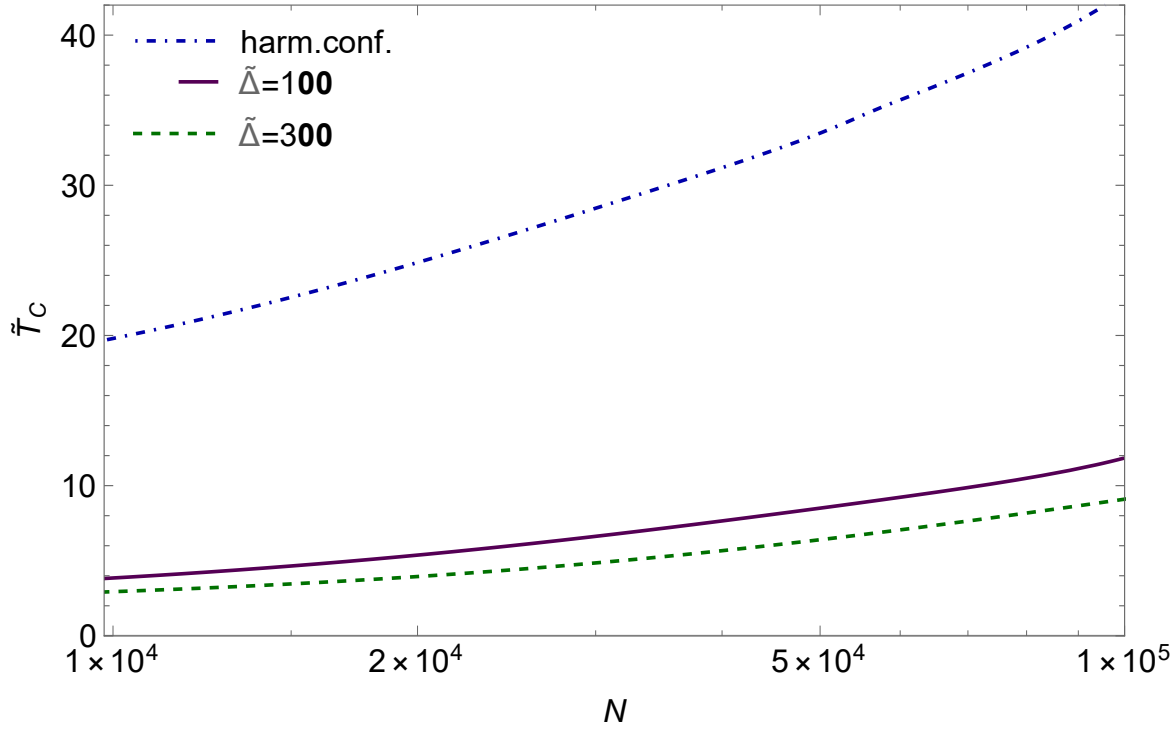

Figure 3.1: Adimensional critical temperature $\tilde{T}_c$ for Bose-Einstein condensation of ^{87}Rb interacting atoms as a function of the total number of atoms N. In the Hartree-Fock approximation that we are considering the bosons behave as a non interacting gas in an effective potential given by Eq.(3.23). In particular the critical temperatures are compared for different external potentials: the adimensional harmonic trap (red line) given by Eq.(1.5), the adimensional bubble-trap potential of Eq.(1.4) with $\tilde{\Omega} = 50$, $\tilde{\Delta} = 100$ (green dashed line) and $\tilde{\Omega} = 50$, $\tilde{\Delta} = 300$ (blue dot-dashed line) Here the temperatures are expressed in unit of the characteristic temperature $T_o = 4.860 \times 10^{-9}$ K and the parameters of the external potential $\tilde{\Delta}$ and $\tilde{\Omega}$ are in units of the characteristic energy $E_0 = 6.632 \times 10^{-32}$K. The characteristic quantities are defined in (1.3)

As we can see from the figure we found results similar to the ones obtained in the previous chapter for the non interacting gas shown in figure 2.8, namely we have that, for a fixed number of atoms N the critical temperature T_c of condensation in the case

in which the gas is trapped in the thinner shell with a bigger size, i.e. when in the bubble-trap potential we set $\tilde{\Delta} = 300$, is slightly lower than the critical temperature in the case of a thicker shell with a smaller size, i.e. when in the bubble-trap potential we set $\tilde{\Delta} = 100$.

Moreover, also in this case we can see that the quantum degeneracy is harder to reach in bubble-traps than in conventional harmonic trap, provided by considering as the external potential the harmonic potential, since for the full filled configuration the critical temperature is much bigger.

Finally, in Fig. 3.2 we compare the results obtained for the dilute interacting Bose gas having total density $\tilde{n}(\tilde{r})$ given by Eq.(3.32) with the ones obtained in the previous section for the non interacting ideal Bose gas having total density given by Eq.(2.14), which is the expression to which the total density of the interacting dilute gas reduces if we set $a_s = 0$, i.e. $g = 0$.

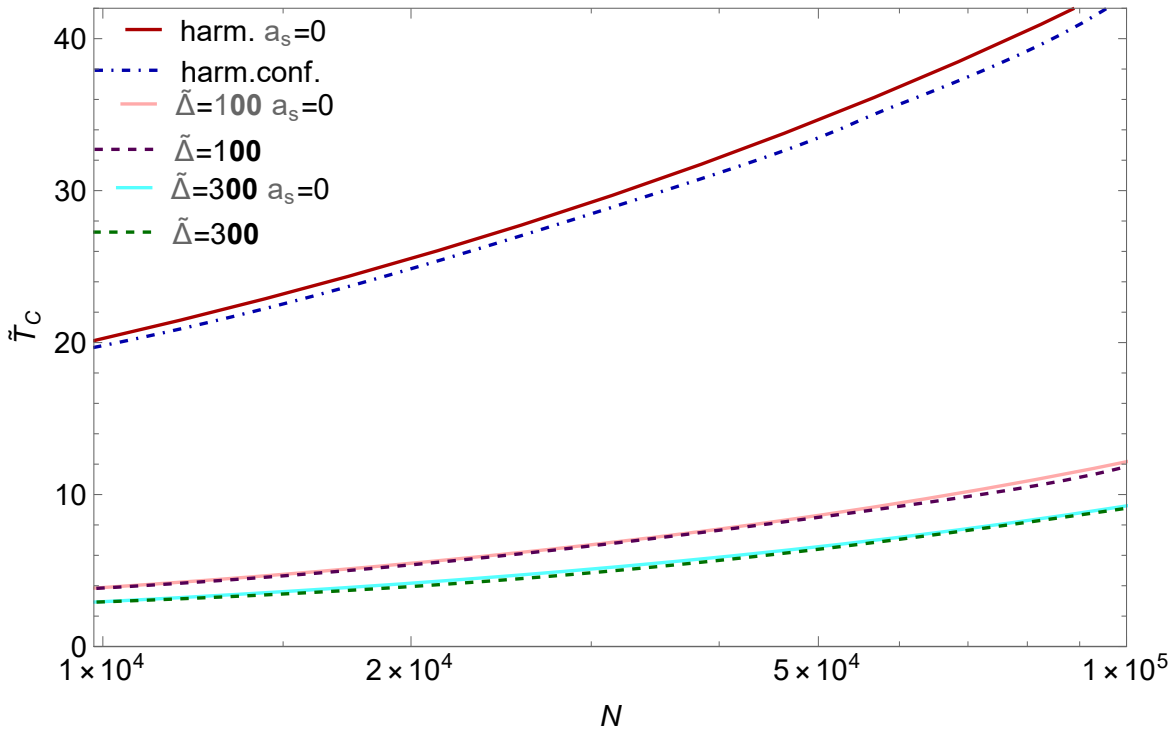

Figure 3.2: Adimensional critical temperature for Bose-Einstein condensation as a function of the total number N of ^{87}Rb atoms. The temperatures are computed considering both the non interacting and the interacting case, then we compare this two cases for different external potential $\tilde{U}(\tilde{r})$: the harmonic potential of Eq.(1.5) obtained setting $\tilde{\Delta} = \tilde{\Omega} = 0$, the bubble-trap potential of Eq.(1.4) with $\tilde{\Omega} = 50$, $\tilde{\Delta} = 100$ and with with $\tilde{\Omega} = 50$ and $\tilde{\Delta} = 300$. The plot are obtained using the Eq.(3.38) in which for the non interacting case we set the mean field $U_{MF}(\vec{r})$, i.e. the scattering length $a_s = 0$, to zero, so that the expression reduces to Eq.(2.20). Here the temperatures are in units of the characteristic temperature $T_0 = 4.860 \times 10^{-9}$ K and the parameters of the external potential $\tilde{\Omega}$ and $\tilde{\Delta}$ are in units of the characteristic energy $E_0 = 6.632 \times 10^{-32}$ J. The characteristic quantities are defined in Eq.(1.3).

As shown in figure 3.2, we found a very slight negative δT_c^{int} shift for the critical temperature of the interacting gas with respect to the one of the non interacting gas.

The presence of a repulsive interaction has the effect of broadening the density distribution, i.e. expanding the atomic cloud [23], this results in a shift of the critical temperature towards lower temperatures which is associate with a change in the central density produced by interatomics forces. In other words, the shift has the following physical interpretation: the presence of repulsive interactions among the atoms acts in reducing the density of particles at the center of the trap $\tilde{n}(\tilde{r}_0)$. Thus lower temperature are needed to reach there the critical density for Bose-Einstein condensation [20].

It is important to note that in the present mean-field approach the relationship between the critical temperature of condensation $\tilde{T}_c$ and the corresponding value of the density in the center of the trap $\tilde{n}(\tilde{r}_0)$ is unaffected by the interaction [26].

This can be seen by looking at the expression of the thermal density of Eq.(3.32) which at the critical temperature $\tilde{T}_c$ gives the total density $\tilde{n}(\tilde{r})$ of the system. We know that the critical chemical potential, $\tilde{\mu}_c = \tilde{\mu}(T_c)$, is equal the minimum of the effective potential $\tilde{U}_{eff}(\tilde{r}_0)$ with minimum point given by $\tilde{r}_0 = 2\sqrt{\tilde{\Delta}}$. Therefore at the center of the trap at $\tilde{r} = \tilde{r}_0$ the argument of the Bose function $g_{3/2}(z)$ is 1 and the central density reduces to $\tilde{n}(\tilde{r}_0) = (\tilde{T}_c/2\pi)^{3/2} g_{3/2}(1)$ which is the same expression it has for the ideal case.

It is possible to estimate the shift δT_c^{int} in the critical temperature due to the presence of the interaction. As said above, for large value of the parameter $\tilde{\Delta}$ the bubble-trap potential $\tilde{U}(\tilde{r})$ of Eq.(1.4) is approximated, near its minimum at $\tilde{r} = \tilde{r}_0$, by a radially shifted harmonic trap potential [10]

$$U_{rad}(\tilde{r}) = \frac{m}{2}\omega_o^2\, l_c^2\, (\tilde{r} - \tilde{r_0})^2 \tag{3.39}$$

For an harmonic trap the critical temperature is shifted due to the presence of the interaction, to lowest order in the coupling constant g, with respect to its ideal gas value T_c^0 by an amount δT_c^{int} given by [26]

$$\frac{\delta T_c^{int}}{T_c^0} \simeq -1.33\, \frac{a_s}{l_0}\, N^{\frac{1}{6}} \tag{3.40}$$

where a_s is the s-scattering length, l_0 is the length of the harmonic confinement and N is the total number of atoms.

As an example let us consider a gas of atoms in a shell-shaped trap, namely confined by the external potential given by the bubble-trap potential $\tilde{U}(\tilde{r})$ of Eq.(1.4) in which we set $\tilde{\Delta} = 100$ and $\tilde{\Omega} = 50$.
Let us suppose that the gas that we are considering has a critical temperature in the non interacting case $T_c^0 = 30$ nK (i.e. $\tilde{T}_c^0 = 6.25$), namely the total number of atoms in the gas is N= 26093. The shift in the critical temperature due of the pres-

ence of the interaction is $\delta T_c^{int} \simeq -1nk$ which in rescaled units becomes $\delta\tilde{T}_c^{int} \simeq -0.2$.

If instead we consider a gas confined by the harmonic potential such to have as the critical temperature in the non interacting case $T_c^0 = 170$ nK (i.e. $\tilde{T}_c^0 = 35$) which corresponds to a gas having $N = 51538$ atoms, the shift in the critical temperature due of the presence of the interaction is $\delta T_c^{int} \simeq -6.33$ nK which in rescaled units becomes $\delta\tilde{T}_c^{int} \simeq -1.3$.

These results are obtained by using the expression of Eq.(3.40) for the shift in the critical temperature and are in agreement with the plot shown in figure 3.2.
Notice that the adimensional temperatures $\tilde{T}$ are in units of the critical temperature $T_0 = 4.860 \times 10^{-9}$ defined in (1.3).

In general, one expects that the deviations from mean-field theory will be important near the transition point T_c. It is possible to show that the leading correction to the critical temperature, due to the presence of the interaction is dominated by the mean-field effect and beyond-MF effects provides only higher- order corrections. This can be understood by noticing that the region affected by the critical behaviour is restricted to a small volume near the centre of the trap. [24]

3.3 Density profiles

A gas of N identical atoms is described by a bosonic field operator $\hat{\Psi}(\vec{r}, t)$ which in the Bogoliubov approximation [28] can be written by separating out the condensate part

$$\hat{\Psi}(\vec{r}, t) = \Phi(\vec{r}) + \hat{\phi}(\vec{r}, t) \tag{3.41}$$

where $\Phi(\vec{r})$ is the order parameter (macroscopic wavefunction) of the condensate $\Phi(\vec{r}) = \langle\hat{\Psi}(\vec{r}, t)\rangle$ normalized to the total number of atoms N_0 in the condensate and $\hat{\phi}(\vec{r}, t)$ represents the fluctuations of the condensate.

In the mean-field Hartee-fock approximation [23] described in the section 3.1, within the semiclassical approximation [20], the order parameter $\Phi(\vec{r})$ satisfies the following finite-temperature Gross-Pitaevskii equation [29, 30]

$$\left[-\frac{\hbar^2}{2m}\nabla^2 + U(\vec{r}) + gn_0(\vec{r}) + 2gn_T(\vec{r}) \right]\Phi(\vec{r}) = \mu\Phi(\vec{r}) \tag{3.42}$$

where $g = 4\pi\hbar^2 a/m$ is the coupling constant , $n_0(\vec{r})$ is the condensate density and $n_T(\vec{r})$ is the thermal density of non-condensed particles. Notice that in this approximation we are ignoring the $T = 0$ quantum depletion [35].

We are considering an interacting gas which is dilute, $\bar{n}a_s^3 \gg 1$ with $\bar{n}$ the average density of the gas, but also strongly interacting since

$$N\frac{a_{s,Rb}}{l_c} \gg 1 \tag{3.43}$$

where $a_{s,Rb} = 50\dot{A}$ is the scattering length and $l_0 = \hbar/m\omega = 1.09 \times 10^{-6}m$ is the characteristic length introduced in (1.3).

The one in Eq.(3.43) is the parameter expressing the importance of the atom-atom interaction compared to the kinetic energy, therefore the kinetic term of the equation (3.7) can be neglected and one gets the Thomas-Fermi approximation in which the condensate density reduces to

$$n_0(\vec{r}) = \frac{1}{g}[\mu - U(\vec{r}) - 2gn_T(\vec{r})] \tag{3.44}$$

in the region where $\mu > U(\vec{r}) + 2gn_T(\vec{r})$ and $n_0(\vec{r}) = 0$ outside.

We found in the previous section that the thermal density $n_T(\vec{r})$, within the Hartree-Fock approximation in which we consider the thermal particles as a gas of non interacting bosons in a self-consistent effective potential $U_{eff}(\vec{r}) = U(\vec{r})+2gn(\vec{r})$, is given by

$$n_T(\vec{r}) = \frac{1}{\lambda_T^3} g_{3/2}\left(e^{(\mu - U(\vec{r}) - 2gn(\vec{r}))/k_BT}\right) \tag{3.45}$$

By substituting the expression of the condensed density $n_0(\vec{r})$ of Eq.(3.44) in the one of the thermal density $n_T(\vec{r})$ of Eq.(3.45) one can obtain a more symmetric form for the thermal density $n_T(\vec{r})$ which does not explicitly depend on $n_0(\vec{r})$ [21]

$$n_T(\vec{r}) = \frac{1}{\lambda_T^3} g_{3/2}\left(e^{-(\mu - U(\vec{r}) - 2gn_T(\vec{r}))/k_BT}\right) \tag{3.46}$$

moreover, since the number of particles N is kept constant the chemical potential μ must satisfy the normalization constraint

$$N = \int d^3\vec{r}\ [n_0(\vec{r}) + n_T(\vec{r})] \tag{3.47}$$

equations (3.44), (3.46) and (3.47) have to be solved simultaneously.

Notice that in the Hartree-Fock approximation that we are considering the spectrum of excitations is given by Eq.(3.24).

Let us now consider a system with a fixed constant number of atoms N to which corresponds a certain critical temperature of condensation T_c.

For a temperature lower than the critical temperature $T < T_c$ we compute the thermal density $n_T(\vec{r})$, by using equation (3.46), in a self-consistent way until convergence is reached. Notice that, as pointed out above, in the expression we employ for the thermal density $n_T(\vec{r})$ the density of the condensate $n_0(\vec{r})$ does not appear. The iterative procedure that we use is analogous to the one we used in the previous section to compute the total density $\tilde{n}(\tilde{r})$ of Eq.(3.46), in that section a more detailed description of the procedure is presented.

Once we have calculated the thermal density in this way, we proceed by computing the condensed density $n_0(\vec{r})$ of equation (3.44) within the Thomas-Fermi approximation and after that we fix the chemical potential μ so that the normalization condition (3.47) is satisfied.

At this point we repeat the procedure to compute the thermal density $n_T(\vec{r})$ using the correct value of the chemical potential μ that we have found from the normalization condition and finally we calculate also the density of the condensate $n_0(\vec{r})$.

Let us consider a gas of $N = 1.6 \times 10^5$ interacting ^{87}Rb atoms in a shell-shaped trap given by the bubble-trap potential $U(\vec{r})$ of Eq.(1.4) in which we set the parameters $\tilde{\Delta} = 100$ and $\tilde{\Omega} = 50$. For such a system the critical temperature of condensation is $T_c = 72$ nK, which in units of the characteristic temperature $T_0 = 4.860 \times 10^{-9}$ K defined in (1.3) becomes $\tilde{T}_c = 15$.

In figure 3.3 we show the adimensional density profiles $\tilde{n}_0(\tilde{r})$ of the condensed particles as a function of the adimensional radius $\tilde{r}$. The condensate density profiles $\tilde{n}_0(\tilde{r})$ are compared for different adimensional temperatures: $\tilde{T} = 13$ (i.e. $T = 62.4$ nK), $\tilde{T} = 11$ (i.e. $T = 52.8$ nK) and $\tilde{T} = 9$ (i.e. $T = 43.7$ nK).

The adimensional condensate density profiles $\tilde{n}_0(\tilde{r})$ are obtained within the Thomas-Fermi approximation using Eq.(3.44) which is computed in the self-consistent way described above.
Note that the expression for the condensate density (3.44) is written by means of the adimensional quantities defined in (1.3) in a similar way to what we did for the ideal gas.

As we can see from the figure the density profile has a maximum at the center of the trap, namely at $\tilde{r} = \tilde{r}_0 = 2\sqrt{\tilde{\Delta}}$, which is the point where the external potential $\tilde{U}(\tilde{r})$, i.e. the bubble-trap potential of Eq.(1.4), is minimum.

The value of the maximum of the density decreases with the temperature accordingly to the fact that for increasing values of the temperature the particles go outside the condensate, moreover for decreasing temperature the region occupied by the condensate gets larger since the density profiles gets wider and the total number of atoms N_0 in the condensate increases.

In figure 3.4 we show the adimensional thermal density $\tilde{n}_T(\tilde{r})$ of Eq.(3.46) as a function of the adimensional radius $\tilde{r}$. Also for the thermal density $\tilde{n}_T(\tilde{r})$ we consider different values of the temperature in order to compare the profiles, we choose the same values considered for the condensate density, namely $\tilde{T} = 13$ (i.e. $T = 62.4$ nK), $\tilde{T} = 11$ (i.e. $T = 52.8$ nK) and $\tilde{T} = 9$ (i.e. $T = 43.7$ nK).

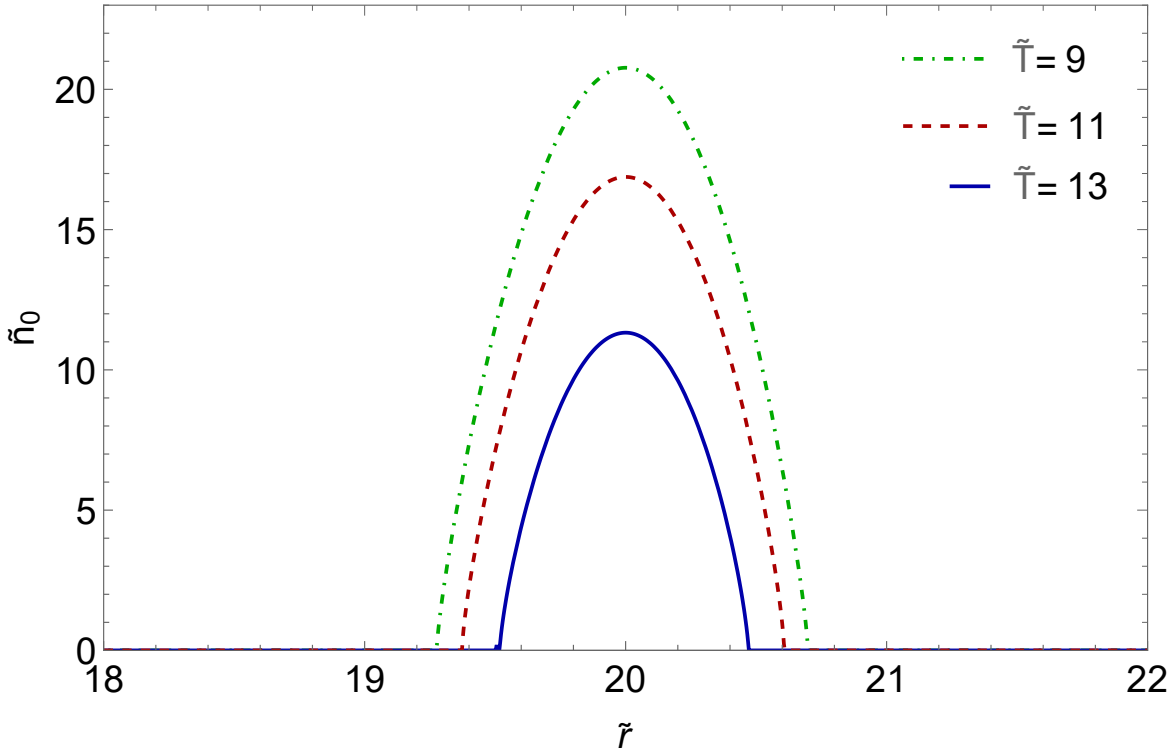

Figure 3.3: Adimensional condensate density profile $\tilde{n}_o(\tilde{r})$ as a function the adimensional radius $\tilde{r}$ for a system of $N = 1.6 \times 10^5$ interacting atoms of ^{87}Rb. The density profiles are compared for different adimensional temperatures: $\tilde{T} = 9$ (green dot-dashed line), $\tilde{T} = 11$ (dashed red line) and $\tilde{T} = 13$ (blue line). The plot are obtained using Eq. (3.44) computed in a self-consistent way in which we consider as the external potential $\tilde{U}(r)$ the bubble-trap potential of Eq.(1.4) with $\tilde{\Delta} = 100$ and $\tilde{\Omega} = 50$ while the thermal density $\tilde{n}_T$ is given by Eq.(3.46). Here the densities are in units of l_0^3 with $l_0 = 1.088 \times 10^{-6}$ m, the radius is in units of l_0 and the parameters of the external potential $\tilde{\Delta}$ and $\tilde{\Omega}$ are in units of $E_0 = 6.632 \times 10^{-32}$ J. Finally, the temperatures are in units of the characteristic temperature $T_0 = 4.860 \times 10^{-9}$, therefore the temperatures that we have considered correspond respectively to $T = 43.7$ nK, 52.8 nK, 62.4 nK. The characteristic quantities are defined in (1.3).

As we can see from the figure the thermal density $\tilde{n}(\tilde{r})$ shows a depletion near the center of the trap, i.e. at $\tilde{r}_0 = 2\sqrt{\tilde{\Delta}}$, which is due to the presence of the condensate fraction in that region, indeed as seen in Fig. 3.3, the condensate density profile $\tilde{n}_0(\tilde{r})$ has its maximum in this region. Moreover we can see that the thermal density profile $\tilde{n}_T(\tilde{r})$ extends in a larger region with respect to the condensed density profile $\tilde{n}_0(\tilde{r})$ which is localized near the center of the trap at $\tilde{r}_0$. Therefore the condensate occupies the internal region of the trap while the thermal component forms a broader cloud as we can see noticing the different abscissae scale.

The adimensional densities $\tilde{n}_T(\tilde{r})$ and $\tilde{n}_0(\tilde{r})$ are in units of l_0^3 where $l_0 = 1.088 \times 10^{-6}$ m is the characteristic length of the system, the adimensional radius $\tilde{r}$ is in unit of l_0, the temperature $\tilde{T}$ are in units of $T_0 = 4.860 \times 10^{-9}$ K and the parameters of the external potential $\tilde{\Delta}$ and $\tilde{\Omega}$ are in units of $E_0 = 6.632 \times 10^{-32}$ J. The characteristic quantities are defined in (1.3).

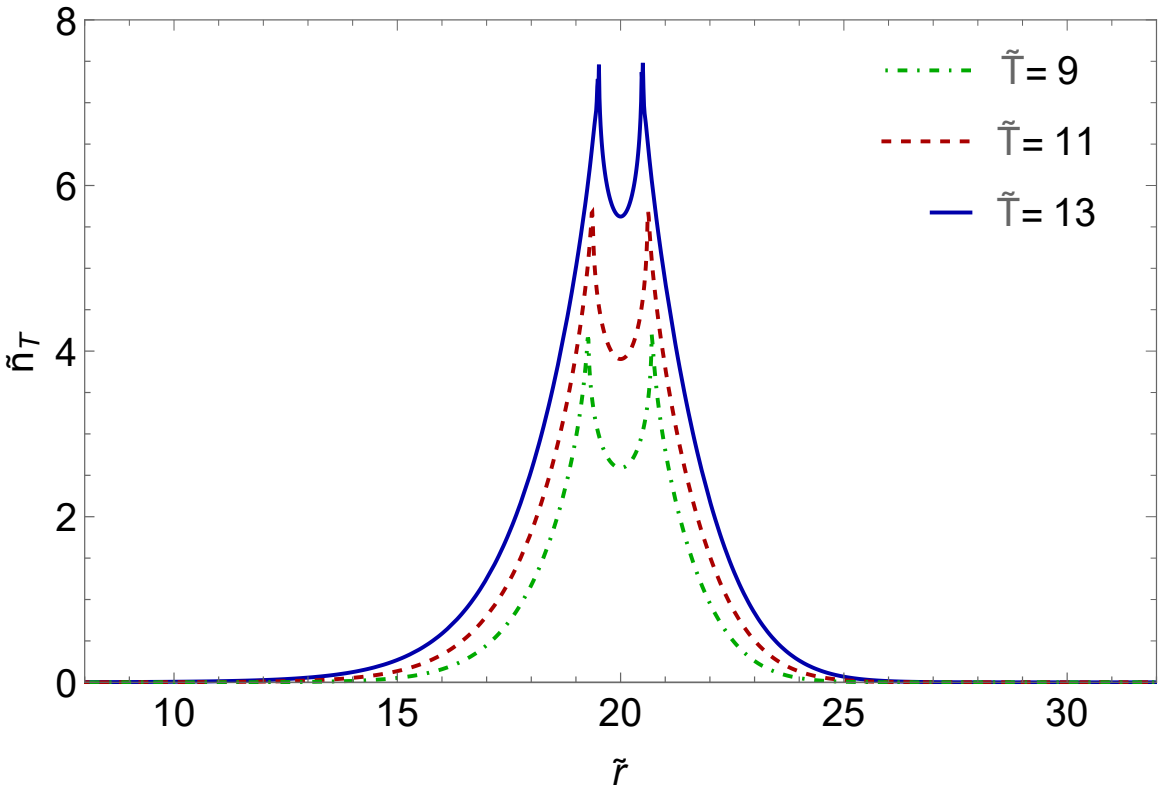

Figure 3.4: Adimensional thermal density profile $\tilde{n}_T(\vec{\tilde{r}})$ as a function of the adimensional radius $\tilde{r}$ for a system of $N = 1.6 \times 10^5$ interacting atoms ^{87}Rb. The density profiles are compared for different effective temperatures $\tilde{T} = 9$ (dot-dashed green line) $\tilde{T} = 11$ (dashed red line) and $\tilde{T} = 13$ (blue line). The plot are obtained using Eq.(3.46) computed in a self-consistent way in which we consider as the external potential $\tilde{U}(r)$ the bubble-trap potential of Eq.(1.4) with $\tilde{\Delta} = 100$ and $\tilde{\Omega} = 50$. Here the densities are in units of l_0^3 with $l_0 = 1.088 \times 10^{-6}$ m, the radius is in units of l_0 the parameters of the external potential $\tilde{\Delta}$ and $\tilde{\Omega}$ are in units of $E_0 = 6.632 \times 10^{-32}$ J. The temperatures are in units of the characteristic temperature $T_0 = 4.860 \times 10^{-9}$, therefore the temperatures that we have considered correspond respectively to $T = 43.7$ nK, $T = 52.8$ nK, 62.4 nK. The characteristic quantities are defined in (1.3).

Let us now represent in Fig. 3.5 the condensate fraction N_0/N as a function of the temperature $\tilde{T}$ for the trapped interacting gas that we are considering, namely having $N = 1.6 \times 10^5$ atoms, corresponding to the adimensional critical temperature of condensation $\tilde{T}_c = 15$.
The total number of condensed particles N_0 is computed by integrating over the space the condensate density $\tilde{n}_0(\tilde{r})$ within the Thomas-Fermi approximation of Eq.(3.3) obtained using the self-consistent procedure described.

Moreover we also compare the results obtained with the ones for the ideal gas (blue line) having the same number of atoms $N = 1.6 \times 10^5$ and trapped in the same configuration provided by the bubble-trap potential $\tilde{U}(\tilde{r})$ of Eq.(1.4) with $\tilde{\Delta} = 100$ and $\tilde{\Omega} = 50$, namely the results shown in Fig. 2.9.
In section 2.3 we have computed the critical temperature of condensation for such an ideal gas and we found that $\tilde{T}_c^0 = 15.32$ which is slightly bigger than the one for the

interacting gas, in agreement to the result of Eq.(3.40).

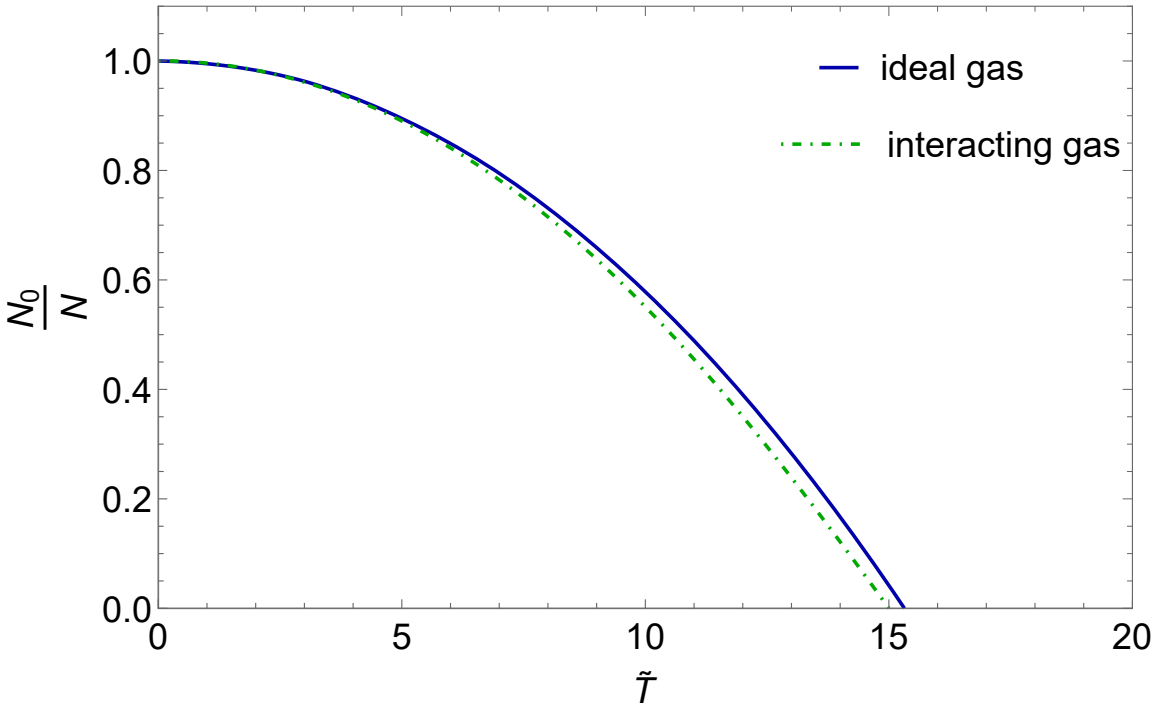

Figure 3.5: Condensate fraction N_0/N as a function of the adimensional temperature $\tilde{T}$. We are considering a gas of $N = 1.6 \times 10^5$ atoms of ^{87}Rb in a shell-shaped trap provided by the bubble-trap potential of Eq.(1.4) with $\tilde{\Delta} = 100$ and $\tilde{\Omega} = 50$. We compare the condensate fraction for the interacting gas (dot-dashed green line) and for an ideal gas (blue line) having the same number of particles N. The total number of atoms N_0 is obtained for the interacting gas by integrating the density $n_0(\vec{r})$ of the condensate given by Eq.(3.44), while for the non interacting case we use the fact that $N_0 = N - N_T$ with N_T computed by integrating over the space the thermal density $n_T(\vec{r})$ of Eq.(2.14). The temperatures are in units of the characteristic temperature $T_0 = 4.860 \times 10^{-9}$ K defined in (1.3).

As we can see from the figure the condensate fraction N_0/N is equal 1 when the temperature is zero $\tilde{T} = 0$ as expected, meaning all the atoms are in the condensate, we are indeed neglecting the quantum depletion at T=0.
For increasing value of the temperature the value of the condensate fraction decreases, going to zero continuously at the critical temperature of condensation $\tilde{T}_c$ where all the atoms are outside the condensate, i.e. $N_0 = 0$.

As shown in the figure the temperature $\tilde{T}_c$ at which the condensate fraction N_0/N for the interacting gas is zero is slightly lower than the one for the ideal gas $\tilde{T}_c^0$, according to what said above.
Moreover the curves in the two cases do not differ much to one another, especially for small values of the temperature $\tilde{T}$, while for increasing values of $\tilde{T}$ the condensed fraction N_0/N for the ideal gas is slightly bigger than the one for the interacting gas.

Finally in Fig. 3.6 we plot the thermal fraction N_T/N as a function of the adimen-

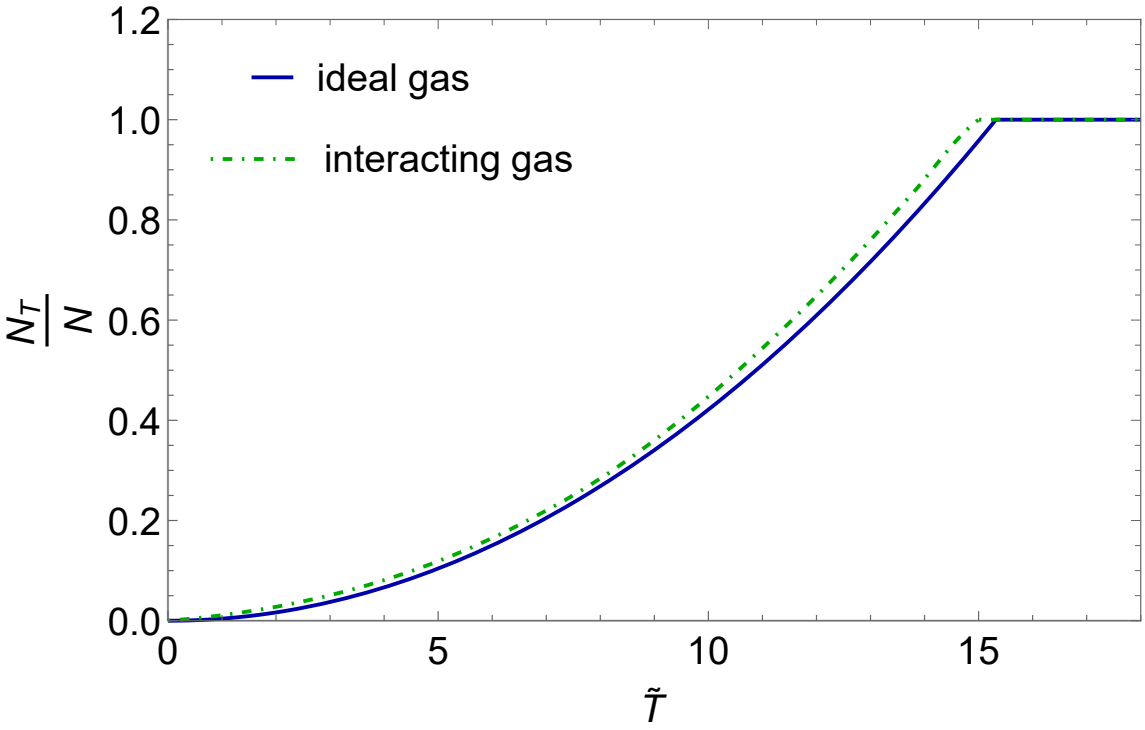

Figure 3.6: Thermal fraction N_T/N as a function of the adimensional temperature $\tilde{T}$. We are considering a gas of $N = 1.6 \times 10^5$ atoms of ^{87}Rb in a shell-shaped trap provided by the bubble-trap potential of Eq.(1.4) with $\tilde{\Delta} = 100$ and $\tilde{\Omega} = 50$. We compare the thermal fraction for the interacting gas (dot-dashed green line) and for an ideal gas (blue line) having the same number of particles N. The total number of atoms N_T is obtained by integrating over the space the thermal density $\tilde{n}_T(\tilde{r})$ which is given by Eq.(2.14)) for the ideal gas and by Eq.(3.46) computed in a self-consistent way for the interacting gas. The temperatures are in units of the characteristic temperature $T_0 = 4.860 \times 10^{-9}$ K defined in (1.3).

sional temperature $\tilde{T}$ for the ideal (blue line) and the interacting case (dot-dashed green line). The total number of atoms N_T is obtained by integrating over the space the thermal density $\tilde{n}_T(\tilde{r})$ which is given by Eq.(2.14) for the ideal gas, while for the interacting gas it is given by Eq.(3.46) which is computed in the self-consistent way described above.

As we can see from the figure the thermal fraction N_T/N is zero when the temperature is zero, $\tilde{T} = 0$, and the values of the fraction increases for increasing values of the temperature until it is equal 1 at the critical temperature $\tilde{T}_c$ and for values of the temperature bigger than $\tilde{T}_c$ when all the atoms are outside the condensate.

Since, as pointed out, for the interacting gas the critical temperature $\tilde{T}_c$ is slightly lower than the one for the ideal gas $\tilde{T}_c^0$, the thermal fraction N_T/N for the interacting gas goes to 1 slightly before than the one for the ideal gas.

Moreover, we can note from the plot that also in this case the curves corresponding to the two different cases do not differ much to one another, in particular this behaviour is more evident for small values of the temperature, while for increasing value of the temperature $\tilde{T}$ the thermal fraction N_T/N for the interacting gas has a

slightly bigger value than the one for the ideal gas.

Conclusions

In this thesis we studied the thermodynamics of bosonic quantum gases on the surface of a sphere motivated by the ongoing project [12] of bubble traps which confine atoms on shells in a microgravity environment.

In the first Chapter we began by analysing the bubble-trap potential which results from an adiabatic deformation of a conventional magnetic trap [15, 16] and depends on two parameters: the detuning Δ of the applied rf field to perform the dressing and the Rabi frequency Ω between two subsequent hyperfine levels.

Our study of this potential consisted in considering different values of the parameters it depends on in order to understand their effects on the shape and the characteristic of the potential. In particular we wanted to understand for which values of the parameters it is possible to achieve a trapping potential shell for the atoms, i.e. a potential where the atoms are confined to the surface of a sphere.

We proceeded by fixing one of the two parameter and we varied the other one and we found that varying the parameter Ω leads to a change in the curvature of the potential in the region near its minimum, in particular the bigger this parameter is the flatter the potential and the dimension of the region in which this behaviour is shown is also controlled by the parameter Ω.

Regarding the detuning Δ we found that it controls the position of the minimum point of the potential which moves away from the origin the more the greater the value of this parameter is. Moreover, for increasing values of the parameter we have a deeper potential well centered at the minimum point.
To compare what we obtained we also considered the harmonic potential, which initially confines the atoms and for which the thermodynamics properties are known.

In the second Chapter we investigated the implication on the density distribution of an ideal gas of ^{87} Rb atoms of the results we had obtained. Namely we considered such a gas in the presence of an external potential given by the ones that we had considered in the previous chapter.
Once we reproduced the expression for the thermal density in the semiclassical approximation that we used throughout the work, we analysed the total density profiles for this gas which is trapped by the various external potential that we had studied. To do so we considered the thermal density at the critical temperature of condensation at which all the atoms are outside the condensate.

As said above we had found that the parameter Ω serves the purpose of controlling the curvature of the potential near its minimum, this action results in a total density profile that is wider for increasing values of this parameter, meaning the atoms are not localized only in the center of the trap but are spread in a bigger region. We showed that the value of the maximum density does not depends on this parameter, hence at a fixed T_c the total number of atoms is bigger for bigger

values of Ω.

In regard of the parameter Δ we found that this has to be much larger than Ω in order to achieve a shell-shaped condensate. Using a realistic value of Ω [12] we indeed found that by varying Δ we are able to pass from a full filled sphere geometry, similar to the one we have with the harmonic potential, to a hollow geometry for bigger values of the parameter, in agreement with [10].

Moreover, it is possible to achieve different trapping configuration from thicker shells with small size (for $\Delta = 100$) to thinner ones with bigger size (for $\Delta = 300$) for increasing value of Δ which hence acts to control the mean radius of the shell-shaped condensate.
Taking into account these results, in the following part we considered this two configuration which allows us to achieve a hollow condensate.

Furthermore, we also investigated the effects on the density profiles of varying the critical temperature and we obtained that the value of the maximum density increases with the temperature and the same happens for the total number of atoms in the gas, consequently also the size of the region occupied by the condensate increases.

To highlight this dependence we calculated the critical temperature as a function of the total number of atoms in the ideal gas. In particular we considered different settings: the smaller thicker shell configuration, the larger thinner shell and, in order to be able to make a comparison, the conventional harmonic trap that is obtained when both parameters are zero and which confines the atoms before the dressing. We found as expected an increase in the critical temperature with the total number of atoms N of the gas and, for fixed N, a strong reduction in T_c for the gas confined in the shell-shaped configuration compared to the harmonic trap having the same confinement frequency. We also found that the critical temperature is slightly lower in the thin shell, in agreement with [22].

Finally, for this ideal gas in a shell-shaped trap, we calculated the fraction of condensate as a function of the temperature which as expected goes continuously to zero at the critical temperature.

Since the results were obtained considering the semiclassical approximation we then explicitly calculated the range of temperatures for which this approximation gives reliable results. To do this we made use of the fact that for large values of Δ we can approximate the bubble-trap potential around its minimum point to an harmonic potential for which we know the condition for the validity of this approximation [24] and we found that this is satisfied for temperatures higher than 9 nK.

We then extended the treatment to the case of an ellipsoidal shell, in particular we considered the case in which there is an axial symmetry and we found similar results to the spherical case. Comparing the results obtained in this two configuration we found that quantum degeneracy is more difficult to reach in the ellipsoidal configuration since the critical temperature is smaller.

At last, in Chapter 3 we considered a dilute strongly interacting gas of ^{87} Rb in a shell-shaped trap provided by the bubble-trap potential. We treated the interaction in the Hartree-Fock theory, following [23], in which we considered the thermal atoms as non interacting bosons in a self-consistent mean field and we consider the Thomas-Fermi approximation which allows us to neglect the kinetic term in the equation for condensate density.

In this context we calculated the total density by adopting a self-consistent iterative procedure and we then calculated the critical temperature as a function of the total number of atoms of the interacting gas trapped in the configurations we had considered in the previous chapter. Afterwards we compared the results obtained with the one for the ideal gas and we found that they are in agreement with what was expected [26], i.e. for a fixed number of atoms in the gas there is a slight decrease of the critical temperature in the interacting case.

In this chapter we then calculated the thermal density at temperatures lower than the critical one, adopting a self-consistent procedure, and we also calculated the condensate density by using the normalization condition to compute the value of the chemical potential. By doing so we saw how the condensate occupies the internal region of the trap while the thermal component forms a broader clouds and it shows a depletion in the region where the condensate is present, i.e. the center of the trap.

Finally we compared the thermal and condensate fraction as a function of the temperature for an ideal and an interacting gas having the same number of atoms and trapped in a shell-shaped configuration having the same value for the parameters. We obtained the typical trend of the condensate and thermal fraction and highlighted the fact that these two gases are characterized by having a different critical temperature.

Bibliography

[1] S.N. Bose, Zeitschrift für Physik **26**, 178 (1924).

[2] A. Einstein, Sitzungsber. K. Preuss. Akad. Wiss., Phys.math. Kl **261** (1924).

[3] A.Einstein Sitzungsber. K. Preuss. Akad. Wiss., Phys.math. Kl **3** (1925)

[4] B.G. Levi, Physics Today **54**, 12 (2001).

[5] E. A. Cornell, C. E. Wieman Rev. Mod. Phys. **74**, 875 (2002).

[6] M. H. Anderson, J. R. Ensher, M. R. Matthews, C. E. Wieman, E. A. Cornell, Science **269**, 198 (1995).

[7] K.B. Davis, M.O. Mewes, M.R. Andrew, N.J. van Druten et al., Phys. Rev. Lett. **75**, 3969 (1995)

[8] C.C. Bradley, C.A. Sackett, J.J. Tollett and R.G. Hulet, Phys. Rev. Lett. **75**, 1687 (1995).

[9] D. Becker, M. D. Lachmann, Ernst M. Rasel et al., Nature **562**, 391 (2018)

[10] K. Sun, K. Padavic, F. Yang, S. Vishveshwara, and C. Lannert, Physical Review A **98**, 013609 (2018).

[11] Z. Hadzibabic, P. Kruger, M. Cheneau, B. Battelier, J. Dalibard, **441**, 1118 (2006).

[12] N. Lundblad, R. A. Carollo, C. Lannert, M. J. Gold, X. Jiang, D. Paseltiner, N. Sergay, D. C. Aveline, npj Microgravity **5**, (2019).

[13] E. R. Elliott, M. C. Krutzik, J. R. Williams, R. J. Thompson , D. C. Aveline, npj Micrograivity **4**, 16 (2018).

[14] D.C. Aveline, J.R. Williams, E.R. Elliott et al., Nature **582**, 193 (2020).

[15] O. Zobay and B. M. Garraway, Phys. Rev. Lett. **86**, 1195 (2001).

[16] O. Zobay and B. M. Garraway Phys. Rev. A **69**, 023605 (2004).

[17] K. Huang, *Statistical Mechanics*, John Wiley Sons, (1963).

[18] S.R. de Groot, G.J. Hooman and C.A. Ten Seldam, Proc. R. Soc. London, Ser. A **203**, 266 (1950)

[19] V. Bagnato, D.E. Pritchard, D. Kleppner, Phys. Rev.A **35**, 4354 (1987)

[20] S. Giorgini, L.P. Pitaevskii, S. Stringari, J. Low Temp. Phys. **109**, 309 (1997)

[21] V.V. Goldman, I.F. Silvera, A. J. Leggett, Phys. Rev. B **24**, 2870(R) (1981)

[22] A. Tononi, F. Cinti, L. Salasnich, Phys. Rev. Lett. **125**, 010402 (2020).

[23] F.Dalfovo, S. Giorgini, L.P. Pitaevskii, Rev. Mod. Phys. **71**, 463 (1999).

[24] L. Pitaevskii, S. Stringari, *Bose-Einstein Condensation and Superfluifity*, Oxford University Press (2016).

[25] R. P. Smith, Z. Hadzibabic, cond-mat/1203.2063 (2012).

[26] S. Giorgini, L. P. Pitaevskii, and S. Stringari, Phys. Rev. A **54** (1996).

[27] A.L. Fetter, J.D. Walecka, *Quantum Theory of Many Particle Systems*, McGraw-Hill (1971).

[28] N. N. Bogolyubov, J. Phys. (USSR) **11**, 23 (1947); Beliaev S T, Sov. Phys. JETP **7**, 299 (1958).

[29] A. Griffin, Phys. Rev. B **53**, 9341 (1996).

[30] E. P. Gross, Nuovo Cimento **20**, 454 (1961); L. P. Pitaevskii, Sov. Phys. JETP **13**, 451 (1961).

[31] V.N. Popov, *Functional integrals and collective excitations*, Cambridge University Press (1987).

[32] H. Shi, G. Varechaka, A. Griffin, Phys. Rev. B **50**, 1119 (1994).

[33] L. Salasnich, cond-mat/0012223 (2001).

[34] D.A. Huse, E.D. Sigga, J. Low Temp. Phys. **46**, 137 (1982)

[35] B. Pozzi, L. Salasnich, A. Parola, L. Reatto, Eur. Phys. J. D **11**, 367 (2000).

[36] C. J. Pethick, H. Smith, *Bose–Einstein Condensation in Dilute Gases*, Cambridge University Press (2008).

[37] L. Salasnich, *Quantum Physics of light and matter*, Springer (2017).